University of Naples Federico II

Department of material and production engineering

PhD in
Materials and Structures Engineering

Cycle XXV

2010-2013

Oxygen Storage Materials: a new type of Hemoglobin Based Oxygen Carrier (HBOC)

Tutor: Prof. P.A. Netti

Candidate: Giuseppe Amalfitano

INDEX

1. Introduction

1.1. State of the art in tissue engineering.

Tissue Engineering is an interdisciplinary field that applies the principles of engineering and life sciences toward the development of biological substitutes that restore, maintain, or improve tissue function or a whole organ. It involves Chemistry, Biology, Bio-Chemistry, Medicine and Engineering with the principle purpose of repairing and replacing portions of whole tissues (i.e., bone cartilage, blood vessels, bladder, skin etc.).

Tissue Engineering utilizes living cells extracted from fluid or solid tissues and categorized by their source:

- Autologous cells are obtained from the same individual to which they will be reimplanted.
- Allogeneic cells come from the body of a donor of the same species.
- Xenogenic cells are these isolated from individuals of another species.
- Syngenic or isogenic cells are isolated from genetically identical organisms.
- Primary cells are from an organism.
- Secondary cells are from a cell bank.
- Stem cells are undifferentiated cells with the ability to divide in culture and give rise to different forms of specialized cells.

In most cases cells are implanted or seeded in a scaffold. A scaffold is a 2D or, in the most cases, a 3D structure mimicking the in vivo milieu and capable to direct cell migration.

Each scaffold must have some fundamental characteristics:

- Biocompatible, biodegradable and bioadsorbable.
- Macrostructure: it must temporary mimic the physiological functions of extracellular matrix (ECM). A model of optimal scaffold should promote cell proliferation and production of a matrix specific to the cells, which

would replace the supportive role of the scaffold after the degradation of the latter.

- Porosity: it must have high porosity with pores opened and interconnected to allow diffusion of nutrients and elimination of waste. It's important to consider that each tissue is different from the other ones so it needs different pores diameter according to the tissue we want to regenerate.
- Mechanical properties: resistance and stability.
- Surface area and surface chemistry: high ratio internal area/volume.
- Workability: it must be workable to allow a possible future scale-up.
- Sterilization: possibility to sterilize it without degradation.

Scaffolds can be realized with various materials and in many different ways. A significant tissue engineering challenge is the development of a competent scaffold for cell cultures with proper mechanical properties to withstand the large contact stresses and strains imposed by micro-environmental conditions, and capability to provide for an appropriate cell-matrix interaction to stimulate functional tissue growth. It has been observed that cell-material interaction influences most processes of cell life. It is well known the importance of biomaterial scaffold in regulating differentiation, tissue growth, and biosynthesis rates of proteins and proteoglycans. In addition biomaterial structures may regulate cellular morphology and therefore may affect differentiation. Indeed the adhesion of cells to their substrate through an extracellular matrix provides signals that influence their ability to survive, proliferate, and express specific developmental phenotypes. Once the cells are implanted or seeded in the scaffold, it must be placed in a bioreactor. A bioreactor in tissue engineering is a device that attends to simulate a physiological environment in order to promote cell or tissue growth in vivo. A physiological environment can consist of many different parameters such as temperature and oxygen or carbon dioxide concentration, but can extend to all kinds of biological, chemical or mechanical stimuli. In

figure 1 the most representative bioreactor for tissue engineering applications are shown:

- Spinner-flask (a) bioreactors have been used for the seeding of cells into 3D scaffolds and for subsequent culture of the constructs . During seeding, cells are transported to and into the scaffold by convection. During culture, medium stirring enhances external mass-transfer but also generates turbulent eddies, which could be detrimental for the development of the tissue.
- Rotating-wall vessels (b) provide a dynamic culture environment to the constructs, with low shear stresses and high mass-transfer rates. The vessel walls are rotated at a rate that enables the drag force (Fd), centrifugal force (Fc) and net gravitational force (Fg) on the construct to be balanced; the construct thus remains in a state of free-fall through the culture medium .
- Hollow-fiber bioreactors (c) can be used to enhance mass transfer during the culture of highly metabolic and sensitive cell types such as hepatocytes. In one configuration, cells are embedded within a gel inside the lumen of permeable hollow fibers and medium is perfused over the exterior surface of the fibers.
- Direct perfusion bioreactors (d) in which medium flows directly through the pores of the scaffold can be used for seeding and/or culturing 3D constructs. During seeding, cells are transported directly into the scaffold pores, yielding a highly uniform cell distribution. During culture, medium flowing through the construct enhances mass transfer not only at the periphery but also within its internal pores.
- Bioreactors that apply controlled mechanical forces (e), such as dynamic compression, to engineered constructs can be used as model systems of tissue development under physiological loading conditions, and to generate functional tissue grafts. Compressive deformation can be applied by a computer-controlled micro-stepper motor.

[1] (fig. 1).

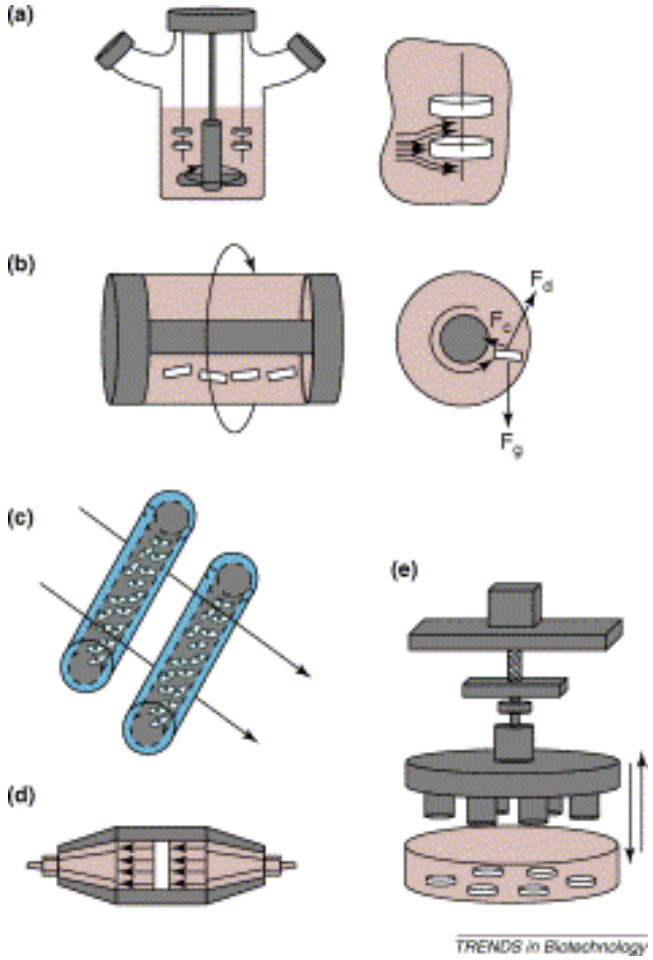

Figure 1 **Representative bioreactors for tissue engineering applications: (a) Spinner-flask bioreactors, (b) Rotating-wall vessels, (c) Hollow-fiber bioreactors, (d) Direct perfusion bioreactors, (e) Bioreactors that apply controlled mechanical forces. [1]**

The construction of scaffolds in regenerative medicine for the realization of in vitro tissues has always been characterized by the death of the cells in the inner parts of the scaffolds with low porosity and static conditions due to the major consumption of nutrients respect to the diffusion [2, 3, 4] (fig. 2). In the other cases (perfusion bioreactors, non-static conditions), when diffusion is equal or faster to nutrients consumption there is a wash out of extracellular matrix [5]. As a consequence, for low porosity

scaffolds in static conditions, the lack of nutrients in the inner zones makes impossible the construction of big and large tissues.

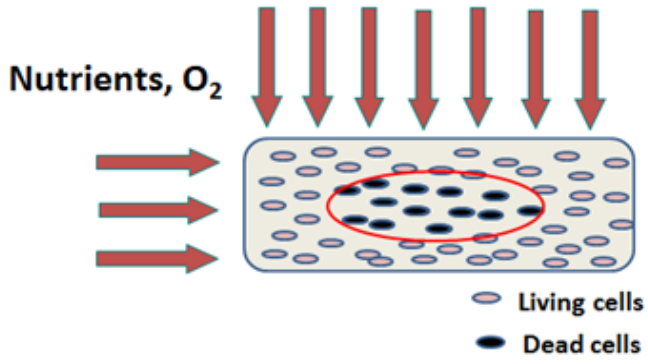

Figure 2 **Death of the cells in the inner parts of the scaffolds with low porosity and diffusion lower than cell consumption**

Molecular oxygen (O_2) is the fundamental nutrient for cell living [6], oxygen gradients are responsible of cellular differentiation [2, 7, 8] and it is the most important regulator of cellular biosynthesis [9].

1.2. Oxygen Carriers.

Different approaches are utilized for the realization of systems that can absorb, carry and release oxygen. PerFluoroCarbons (PFCs) and Hemoglobin Based Oxygen Carriers (HBOCs) are the most common ones, but there are some studies in which other types of systems are used.

1.2.1. Generic oxygen generating materials.

As stated before, PFCs and HBOCs are not the only system utilized for oxygen release. There are some recent studies in which alternative materials are used for this purpose.

For example, in a recent study implantable oxygen generating biomaterial were prepared and tested to determine if they could extend the viability of tissue experiencing hypoxia. The oxygen producing element in the film of Poly(d,l-lactide–co–glycolide) (PLGA) was sodium percarbonate (SPO). It is an adduct of hydrogen peroxide and sodium bicarbonate which spontaneously decomposes upon contact with water to produce oxygen according to the following chemical equation:

$$[Na_2CO_3]_2 \quad X \quad 3H_2O_2 \rightarrow \quad 2Na^+ + 2CO_3^{-2} + 3H_2O_2$$

$$2H_2O_2 \quad \rightarrow \quad O_2 + 2H_2O$$

120mL (at 37 °C) of oxygen can be generated per gram of SPO (fig. 3).

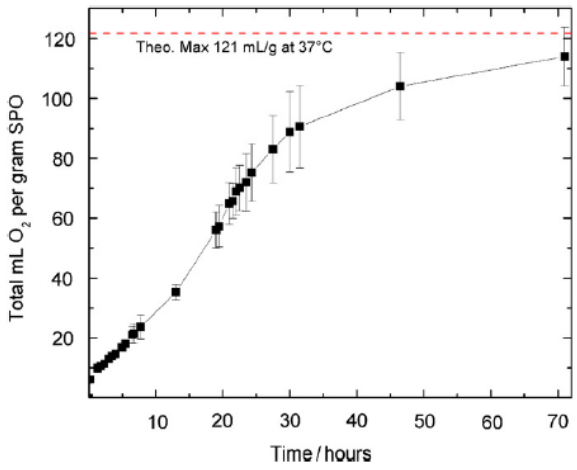

Figure 3 **Oxygen generated from POG Film, in vitro. [10]**

A u-shaped flap was placed in the backs of mice, which reduced the intact vascularity to the 1 cm wide base causing ischemia in the flap. On a tissue level, it became apparent for the non-oxygen producing films that the tissue became necrotic in appearance. Mice, which had the films containing polymeric oxygen generating (POG), had a significantly reduced amount of visible necrosis at days 2 and 3. By day 7, the tissue became necrotic in

appearance similar to the control mice. Histological analysis of the tissue showed significant degradation by day 7 in both films. However, the tissue in contact with the oxygen producing films showed less tissue architecture decay at day 7 compared to the control films with remaining defined layers and intact hair follicles. With oxygen being generated for only the first 24 h after implantation, it is to be expected that the benefit from oxygen generation would only be observed during the first couple of days. The increase is attributed to the existence of loose, non-directional van der Waals interactions leading to low cohesive energy densities, which facilitates mutual solubilization of oxygen in the fluorine compound bound to the surface of the particles that are embedded in the scaffold. This study suggests an increase in cell number for PCU-FZ scaffolds for up to 7 days culture. Cell proliferation on the PCU-FZ scaffolds was significantly higher than on control PCU scaffolds and cell infiltration depths into the PCU-FZ scaffolds were double those into PCU scaffolds. [10]

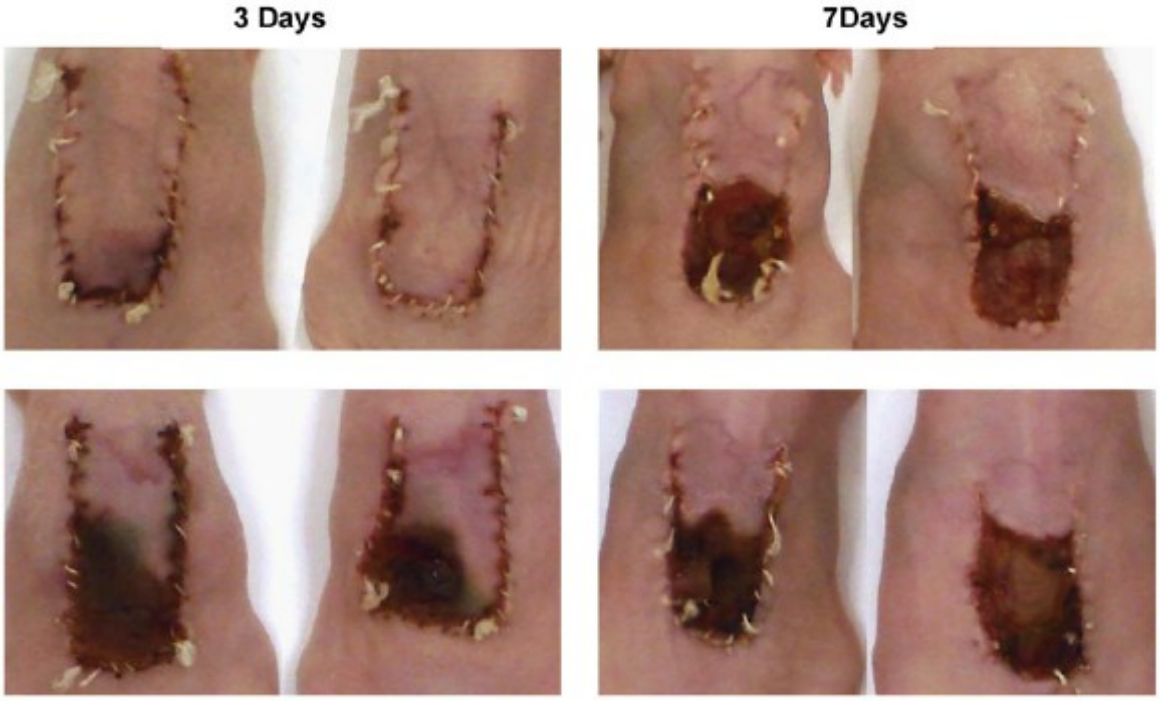

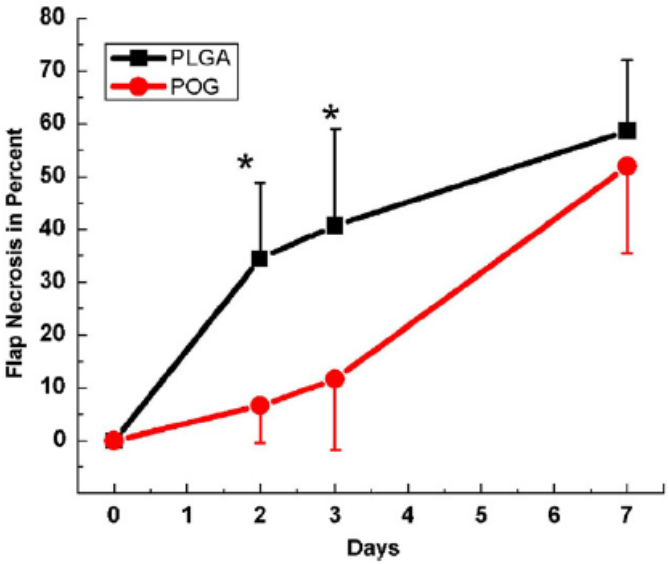

Figure 4 **Flap necrosis. Representative images of study (POG) and control (PLGA) group at 3 and 7 days demonstrating a survival benefit for the polymeric oxygen generating films group in the early time point. The graph expresses the percent necrosis of the total flap size. At early time points, 2 and 3 days, the POG group showed a significant better flap survival with less necrosis, when compared to the control group. However, after 7 days the area of necrosis was similar in both groups. [10]**

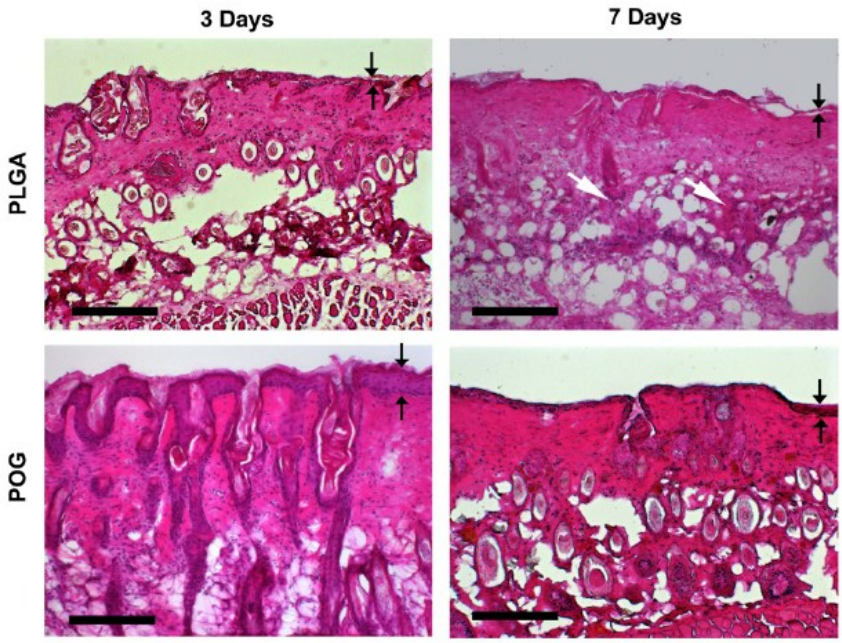

Figure 5 **Histological analysis, 100X: hematoxylin and eosin stains of the skin flaps harvested at 3 and 7 days showed delayed necrosis in the POG group with better conservation of tissue architecture, epidermis height (black arrows), hair follicles and sebaceous glands. Differences were more prominent at the 7 day time point (white arrows show necrotic hair follicles). The size bar represents 500 μm.** [10]

In 2009 Se Heang Oh et al. published a work in which the oxygen generating material is calcium peroxide (CPO). Cylindrical PLGA/CPO scaffolds (diameter 10 mm and height 4 mm) were prepared with a particulate-leaching method using paraffin particles as a porogen. Initial characterization of the scaffolds with SEM showed a highly porous and open-cellular pore structure. Scaffold porosity was about 90%. The scaffolds became stiffer with increasing CPO concentrations. While this trend could be explained by the filler effect caused by particles of CPO, the changes were not significant between different scaffold compositions. When CPO containing scaffolds are placed into water, over time small bubbles of oxygen can be observed forming on the exterior of the scaffold. To quantify the length of time that CPO scaffolds can generate oxygen, dissolved oxygen within the media was measured over a period of 10 days. The scaffolds were maintained under 1% oxygen to mimic hypoxic conditions. When the oxygen generating

scaffold was placed in the media, a small but statistically significant ($p<0.001$) amount of oxygen was produced. A relatively uniform elevation of oxygen levels was observed over a period of at least 10 days. In addition, the pH within the solution remained between 7.2 and 7.6 throughout the experiment.

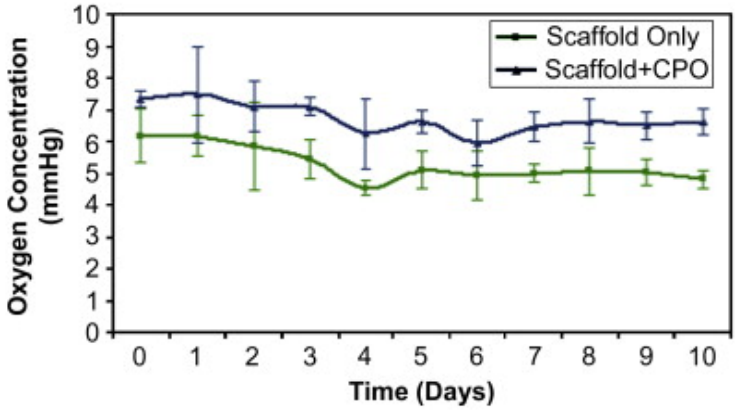

Figure 6 **Oxygen generating behavior of 3-D scaffolds. The media surrounding the oxygen generating scaffolds showed significantly elevated oxygen levels compared to the control when incubated under hypoxic conditions (0.5% O2, 5% CO2, 37 _C) An equal volume of media without the oxygen generating scaffold was used as a control. The standard error of the mean was calculated for each time point with n= 3. [11]**

Calcium peroxide was used to generate oxygen within the scaffold to maintain viability over a period of several days. When it comes in contact with water, it decomposes according to the following chemical equations:

$$CaO_2 + 2H_2O \rightarrow Ca(OH)_2 + H_2O_2$$

$$2H_2O_2 \rightarrow O_2 + 2H_2O$$

Residual reactive oxygen species may be present. So, catalase was added to the media to ensure the decomposition of any hydrogen peroxide byproducts generated. Catalase was added directly to the media for

convenience; however, for in vivo applications, one could envision incorporating catalase or other anti-oxidants directly into the biomaterial [11].

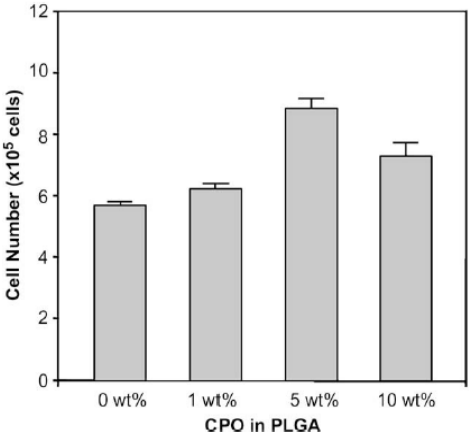

Figure 7 **Cell number of 3T3 fibroblasts grown on oxygen generating 3-D scaffold as a function of CPO wt% in PLGA. One million fibroblasts were seeded onto the scaffolds and cultured under normal culture conditions (21% O2, 5% CO2, 37 _C) for 3 days followed by a MTS assay (n=3, standard error shown) Scaffolds containing 5 wt% CPO showed a significantly higher (P > 0.05) cell count compared to the controls. [11]**

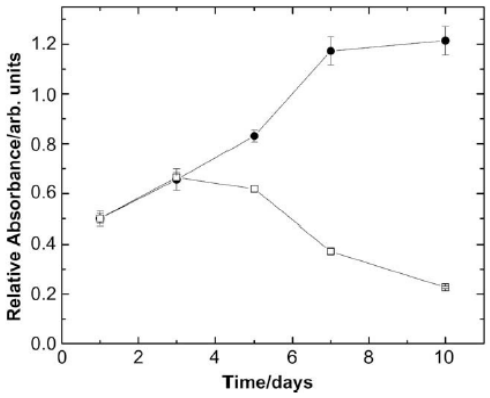

Figure 8 **3T3 Fibroblasts when incubated at 1% oxygen in oxygenating scaffold. Cells cultured at 1% oxygen on the 5 wt% CPO/PLGA (C) and PLGA only (,) scaffolds and were assessed using MTS assays over time (n ¼ 3). After 3 days the CPO containing scaffolds showed increased cell activity compared to controls. [11]**

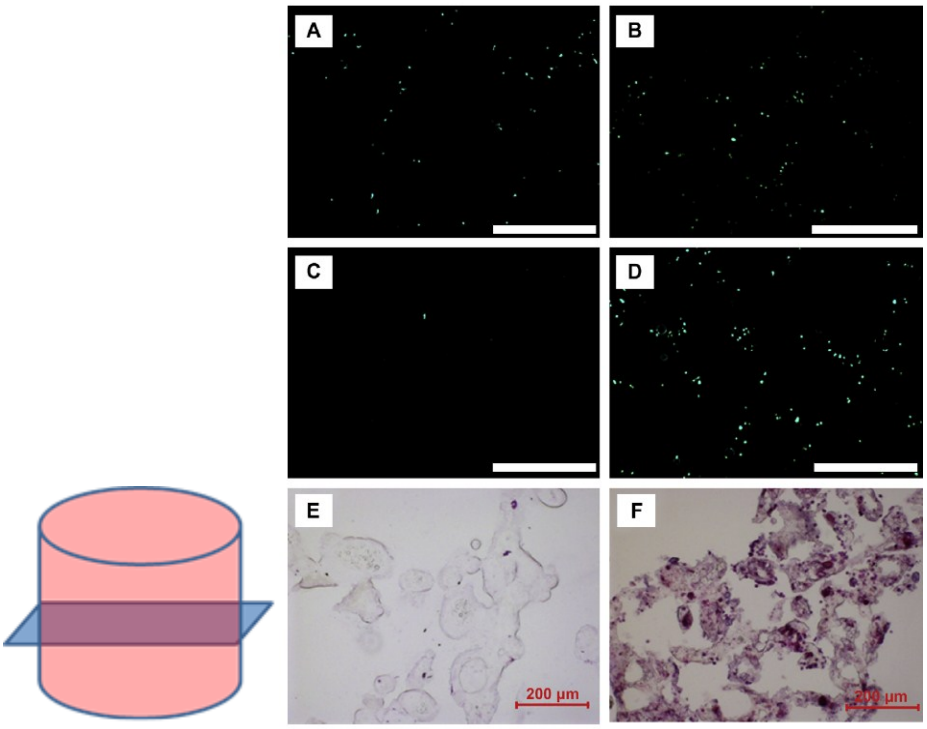

Figure 9 **Cells were stained with DAPI to visualize nuclear morphology on the scaffold: (A) PLGA control day 1; (B) 5 wt% CPO/PLGA scaffold day 1; (C) PLGA control day 10; (D) 5 wt% CPO/PLGA scaffold day 10. The seeded cells show homogeneous distribution in scaffolds (1 day) and the cells are much better grown in PLGA/CPO (5 wt%) scaffold than PLGA scaffold (10 days). Demonstration of the morphology with H&E stain of transversal sections of also shows that after 2 weeks (E) few cells in the PLGA only scaffold and (F) numerous cells in the 5 wt% CPO/PLGA scaffold. Scale bar on DAPI staining is 500 µm. The scale bar on H&E images is 200 µm. [11]**

In a study published in 2011 a novel approach to enhanced oxygen delivery to cells seeded in 3-D scaffolds by incorporating fluorinated porous zeolite particles as an integral part of the scaffolds is proposed. Porous fluorinated zeolite particles with a pore size of 7.4 Å and surface area of $750 m^2 g^{-1}$ were realized and fluorinated with a methanol solution of hydrolyzed 1 wt.% 1H,1H,2H,2H-perfluorodecyltriethoxysilane (PTES).

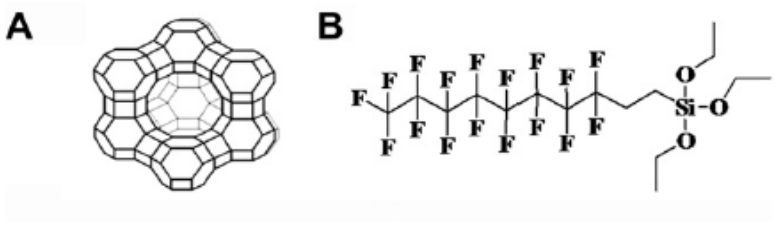

Figure 10 **(A) Framework structure of zeolite Y, (B) chemical structure of PTES. [12]**

A NeoFox fiber optic oxygen sensor (Ocean Optics, Dunedin, FL) equipped with NeoFox software was used to measure dissolved oxygen. The sensor uses ruthenium(II) complexes suspended in a support matrix and attached to the tip of the fiber optic cable. When excited by a light-emitting diode at 475 nm the ruthenium complex fluoresces, with emission at 620 nm. When the excited ruthenium complex encounters an oxygen molecule the emission is quenched, allowing the intensity of the fluorescence to be related to the oxygen concentration. Accordingly, the more oxygen present the lower the emission intensity, and vice versa. In the absence of oxygen the maximum fluorescent intensity of emitted light is observed. FZ particles at concentrations of 0.5%, 1%, and 2% were suspended in deionized water and continuously stirred at 37 °C while the assembly was left open to atmospheric air. Deionized water and non-fluorinated zeolite particles (non-FZ) suspended in deionized water (at 2% concentration) were used as controls. A 300 nm diameter oxygen probe was used to measure the dissolved oxygen following a two point calibration with 20.9% oxygen at standard temperature and pressure and 0% oxygen in 100% nitrogen. The results show that by incorporating 2% FZ in deionized water there was a significant increase in dissolved oxygen at 37 °C. On the other hand, when non-fluorinated zeolite particles were suspended in deionized water there was no difference in the amount of dissolved oxygen compared with deionized water alone. 73% of the fluorinated molecules capable of dissolving oxygen were localized on the surface of the zeolite particles which, in turn, were exposed to the bulk liquid.

This is in contrast to conventional fluorinated emulsions, where the oxygen is trapped in the core of the particle. Consequently, the probe measures total dissolved oxygen concentrations in the system. In view of this, the increased oxygen concentration is attributed to the presence of PTES at the surface of the zeolite particles. Gases are transported by perfluorinated compounds due to increased solubility in accordance with Henry's law.

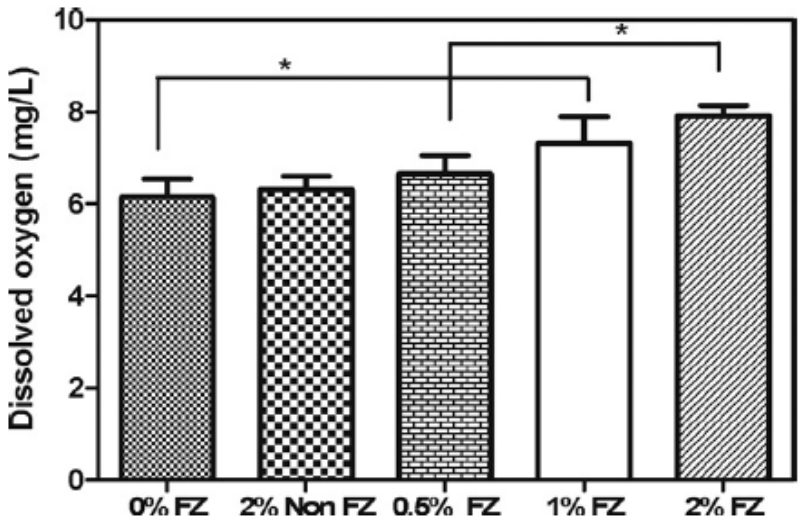

Figure 11 **Dissolved oxygen concentrations in deionized water at 37° C, in the presence of non-fluorinated zeolite particles, and in the presence of different weight percentages of fluorinated zeolite particles. Oxygen concentrations were measured using a fiber optics probe. Data are means ± SD for experiments conducted in triplicate. [12]**

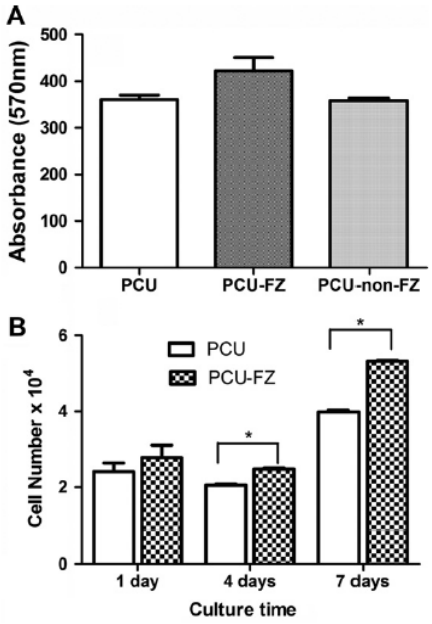

Figure 12 **Human coronary artery smooth muscle cell (HCASMC) (A) viability and (B) growth on PCU, PCU-FZ, and PCU-non-FZ 3-D scaffolds. Data are means ± SD for experiments conducted in triplicate. *Statistical significance. [12]**

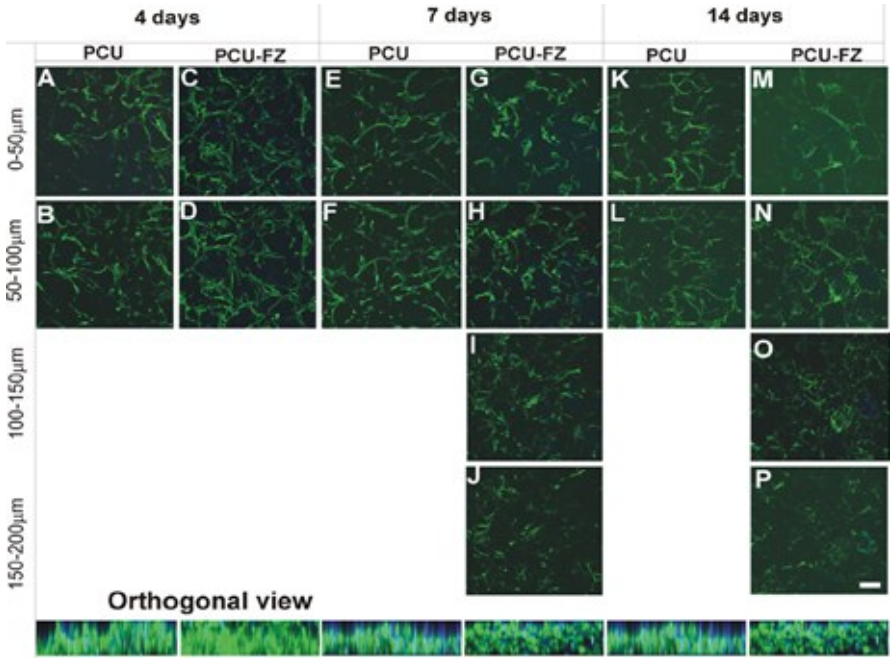

Figure 13 **The effect of FZ incorporation on HCASMC spreading and infiltration after 4, 7 and 14 days of culture. (A, B, E, F, K, L) PCU scaffolds; (C, D, G-J, M-P) PCU-FZ scaffolds. Orthogonal views of the confocal images are shown at the bottom. Scale bar: 200 μm. [12]**

The increase is attributed to the existence of loose, non-directional van der Waals interactions leading to low cohesive energy densities, which facilitates mutual solubilization of oxygen in the fluorine compound bound to the surface of the particles that are embedded in the scaffold.

This study suggests an increase in cell number for PCU-FZ scaffolds for up to 7 days culture.

Cell proliferation on the PCU-FZ scaffolds was significantly higher than on control PCU scaffolds and cell infiltration depths into the PCU-FZ scaffolds were double those into PCU scaffolds [12].

1.2.2. Perfluorocarbons.

One of the basic approaches utilized for oxygen carrier realization consists of perfluorocarbons (PFCs), chemical compounds which can carry and release oxygen. PFCs are low-molecular-weight (450-500 Da) hyper-fluorinated hydrocarbons [13]. The hyperfluorination warrants chemical inertness and complete lack of metabolism in vivo. The PFCs are dense, colorless liquids, with a gas-dissolving capacity (15 to 20 fold that of water) linearly related to the partial pressure of the gas. In 1966 it was demonstrated that a rat immersed in a solution of PFC saturated with oxygen at atmospheric pressure breathed normally. This experience gave rise to the use of PFCs as blood substitutes. Numerous PFCs were synthesized and evaluated as oxygen carriers. As they are chemically and biologically inert, they are not metabolized and are excreted as vapors by the lungs. However, they are immiscible in water and need to be emulsified for intravenous use. The properties and stability of these emulsions depend on the nature and the relative proportions of the components of the emulsion, the sizes and the electric charges of the particles, the surface area available for gas exchange, the viscosity, and the intravascular half-life [14, 15].

The first-generation PFC emulsion authorized in humans was Fluosol-DA®, a 20% w/v solution of two PFCs with a synthetic emulsifying agent. Its limitations were a low concentration and long tissue retention of the PFC components, a limited intravascular half-life, an unsatisfactory stability and biological side effects attributed to the surfactant [16, 17].

Oxygent™ (Alliance Pharmaceutical Corp., San Diego, CA) is a typical example of the second generation emulsions. It is based on perfluorooctyl bromide (perflubron), a linear perfluorocarbon with eight carbon atoms and a terminal bromine atom, which lends lipophilicity and limits tissue persistence. The emulsion is 60% w/v perflubron with egg-yolk phospholipids as an emulsifier, has a median particle diameter of 0.16 to 0.18 μm and a shelf-life of up to 2 years at 2 to 8°C. Oxygent™ dissolves 28 mL oxygen/100 g at 37°C and 750 mm Hg, with a circulating half-life above nine hours for doses around 1.8 g perflubron/kg [15, 18]. Second generation emulsions have higher PFC concentrations, are stable and have a "ready-for-use" formulation in buffered saline with physiological osmolarity, viscosity, and pH values. They have a small size that permit them to be concentrated in the thin layer of the plasma between the red blood cells and the vascular wall and to easily maintain perfusion of all the capillaries of the microcirculation during local vasoconstriction and ischemia [19].

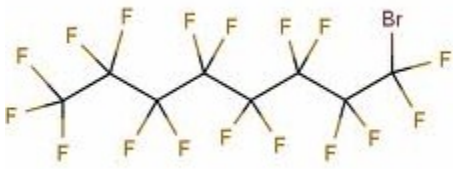

Figure 14 Chemical formula of Oxygent™

1.2.3. Hemoglobin based oxygen carriers (HBOCs)

The other basic approach utilized for oxygen carrier realization consists of hemoglobin (Hb).

Hemoglobin (Hb) is the natural oxygen carrier in all vertebrates and in some invertebrates. In mammals the protein makes up about 97% of the red blood cells' dry content, and around 35% of the total content (including water). Hemoglobin has an oxygen binding capacity of 1.34 ml O_2 per gram.

It is an allosteric protein with a diameter of 55 angstrom. As shown in figure 15, it is a tetramer composed of two types of subunits designated α and β, with stoichiometry α2β2. The four subunits of hemoglobin sit roughly at the corners of a tetrahedron, facing each other across a cavity at the center of the molecule. Each of the subunits contains a heme prosthetic group. The heme molecules give hemoglobin its red color that is the typical color of the red blood cells too. Each individual heme molecule contains one Fe^{2+} atom.

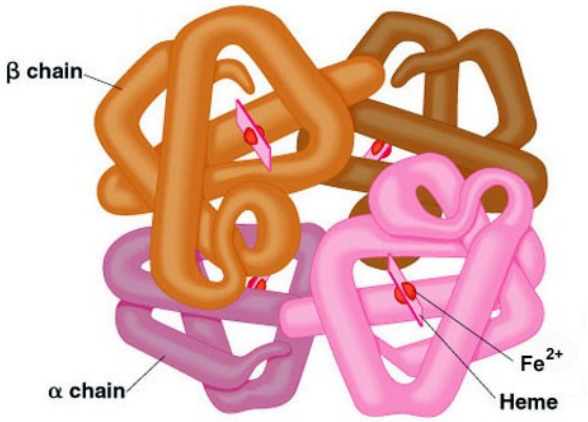

Figure 15 **Quaternary structure of hemoglobin.**

In the lungs, where oxygen is abundant, an oxygen molecule binds to the ferrous iron atom of the heme molecule and is later released in tissues needing oxygen. The heme group binds oxygen while still attached to

the hemoglobin monomer and the oxygenated heme group is held within the polypeptide.

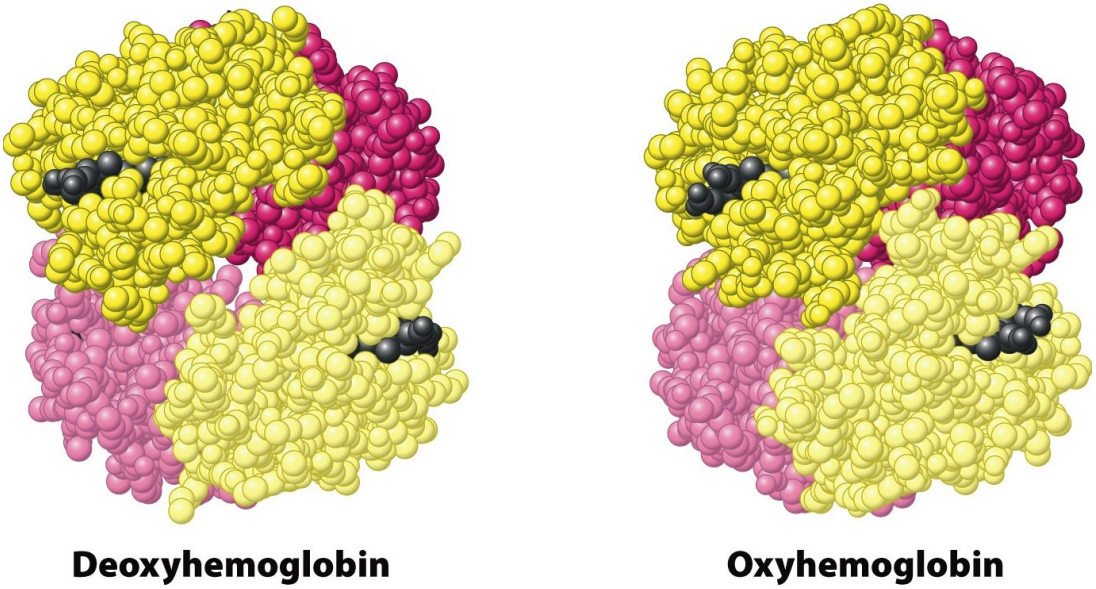

Figure 16 **Hemoglobin in deoxy (left) and in oxy (right) form. Source: Biochemistry; Seventh Edition, © 2012 W.H. Freeman and Company**

Anchoring of the heme is facilitated by a specific histidine nitrogen that binds to the iron. A second histidine is near the bound oxygen. The "arms" (propanoate groups) of the heme are hydrophilic and face the surface of the protein while the hydrophobic portions of the heme are buried among the hydrophobic amino acids of the protein. For hemoglobin, its function as an oxygen-carrier in the blood is fundamentally linked to the equilibrium between the two main states of its quaternary structure, the unbound "deoxy" or "T state" versus the bound "oxy" or "R state" (figure 16). The unbound (deoxy) form is called the T (for "tense") state because it contains extra stabilizing interactions between the subunits. In the high-affinity R state conformation the interactions which oppose oxygen binding and stabilize the tetramer are "relaxed". Structural changes occur during this transition and they result in important functional properties, such as cooperativity of oxygen binding and allosteric control by pH (figure 17) and anions. O_2 release

increases in the presence of H^+ (metabolically active tissues). In fact, hydrogen ions bind to hemoglobin and decrease the affinity for O_2. Therefore the release can be also modulated by a change in pH. Carbon dioxide instead binds strongly and reversibly to the heme group, increasing the affinity of Hb for oxygen. Therefore it's unfavorable for O2 release to tissues. The cooperative binding by Hb is also regulated by a molecule called bisphosphoglicerate (BPG), present in higher concentrations in smokers and those who live in high mountains. Its role is to stabilize the deoxy form resulting in greater delivery of oxygen. The oxygen saturation of hemoglobin varies greatly depending on the different tissues (it is high in the capillaries and low in muscles under stress conditions).

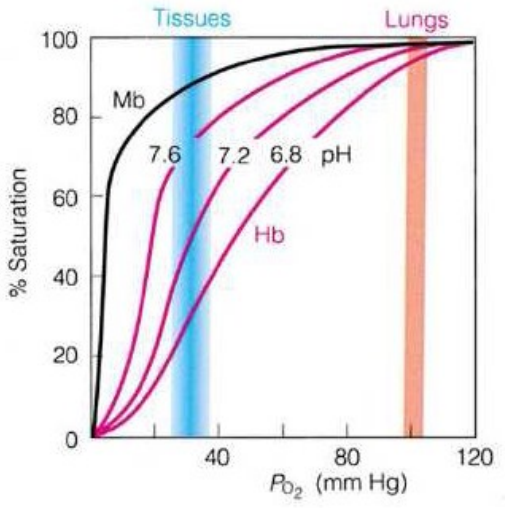

Figure 17 **Cooperative effect on hemoglobin and allosteric control by pH.**

Hb is derived from humans, animals, or artificially via recombinant technology and it is used free or conjugated to some molecules (Hemoglobin Based Oxygen Carriers, HBOCs) [20].

Free hemoglobin solutions are able to transport oxygen but Hb crosses into the extravascular spaces, where it could interact with nitric oxide and lead to vasoconstriction [21, 22]. To avoid this collateral effect, synthetic or

semi-synthetic preparations of Hb, called Hemoglobin Based Oxygen Carriers (HBOCs), were realized in last several decades as an alternative to Red Blood Cells (RBCs).

Various studies demonstrated that Hb can bind to functionalized and non-functionalized carbon nanotube [23]. Besides it can be immobilized on modified zirconia nanoparticles-grafted collagen matrix [24] or on gold nanoparticles stabilized by chitosan [25]. It can also be encapsulated in ordered mesoporous silicas or bound to polyethylene glycol (PEG) through carbodiimide chemistry as shown in fig.18 [26]. In this last case hemoglobin were cross-linked with difunctional polyethylene glycol (PEG) and coencapsulated with pancreatic islets in alginate–poly-L-lysine microcapsules.

A five-layers membrane (fig 19) effectively prevented the loss of Hb-C for at least 8 week. The results of in vitro longterm culture (8 weeks) of the capsules at a glucose concentration of 300 mg/dL and PO2 40 mmHg demonstrated improved islet viability of 380% and enhanced insulin secretion up to 550% compared with the control (without Hb-C).

The results may be attributed to various potential roles of Hb-C, but primarily rely on facilitated oxygen transport under the tested experimental conditions and strongly support the idea that the introduction of Hb-C in a biohybrid artificial pancreas (BAP) may decrease the number of islets required to maintain normoglycemia and possibly increase the lifespan of the BAP after implantation. [26]

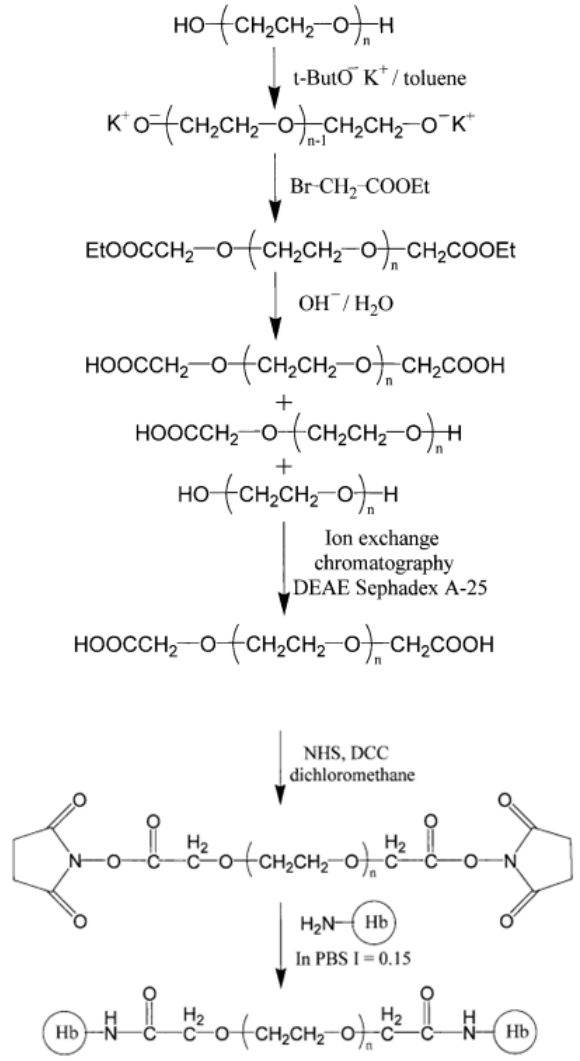

Figura 18 **Dicarboxylation of PEG (The hydroxy groups of both PEG ends were converted to an activated form ($–O^-K^+$) and reacted with ethyl bromoacetate. The ethyl protection groups were removed by hydrolysis and pure PEG diacid was obtained by ion-exchange chromatography) and activation of dicarboxylated PEG by dicyclohexyl carbodiimide (DCC) and N-hydroxy succinimide (NHS) and conjugation of hemoglobin with activated PEG. [26]**

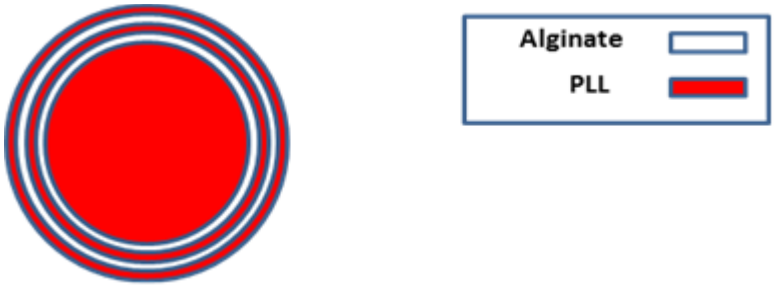

Figure 19 **Scheme of PLL-Alginate five layers membrane**

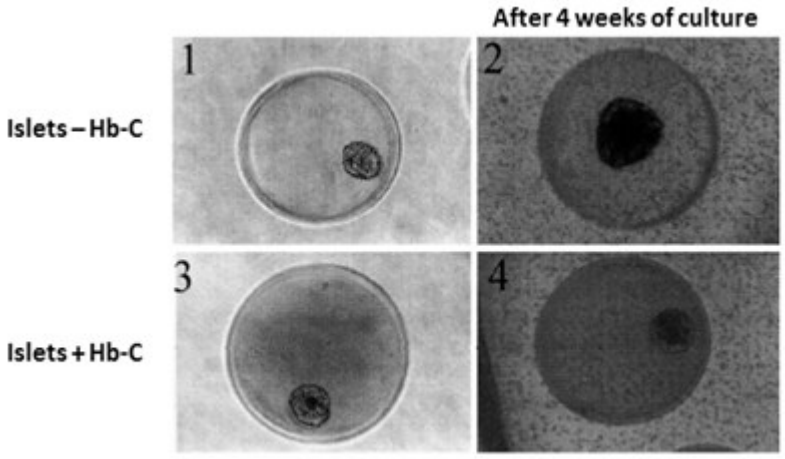

Figura 20 **Photographs of islet microcapsules showing different degrees of islet central necrosis. (1) Control (without Hb-C) islet after encapsulation; (2) control islet after 4 weeks of culture at PO2 = 40 mmHg; (3) islet with Hb-C after encapsulation; and (4) islet with Hb-C after 4 weeks of culture at PO2 = 40 mmHg. [26]**

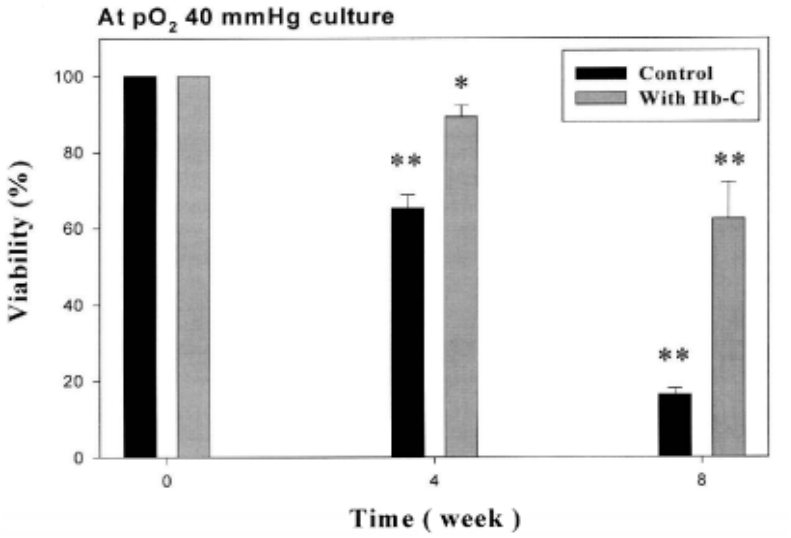

Figure 21 **Islet viability of statically cultured islets. Islet viability was calculated as a percentage of the viable cell volume: [(total volume - necrotic core volume)/total volume] * 100. The data are expressed as means ± SD (n = 5) and the p values were obtained by unpaired Student t test (*p < 0.01, **p < 0.005 compared with week 0 data). [26]**

Among the blood-cell substitutes developed up to date, hemoglobin vesicles (HbV), prepared by encapsulating hemoglobin (Hb) molecules into lipid or polymeric vesicles, exhibit much better performance than chemically

modified Hbs [27]. In most cases, HbVs need to be modified with PEG to guarantee long storage time, blood compatibility and extended circle life.

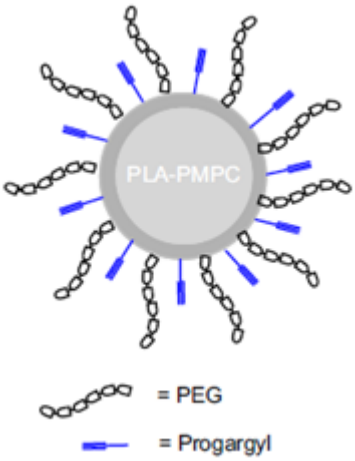

Figura 22 **Scheme of a micelle formed from PML copolymers**

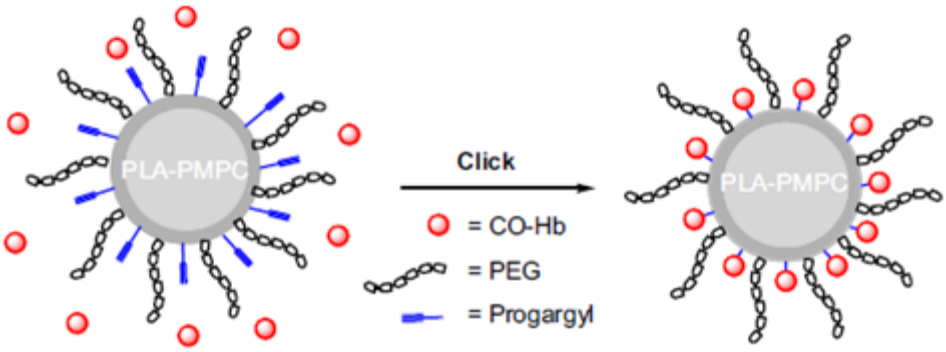

Figure 23 **Conjugation of CO-Hb to the core of PML micelle via click chemistry. [28]**

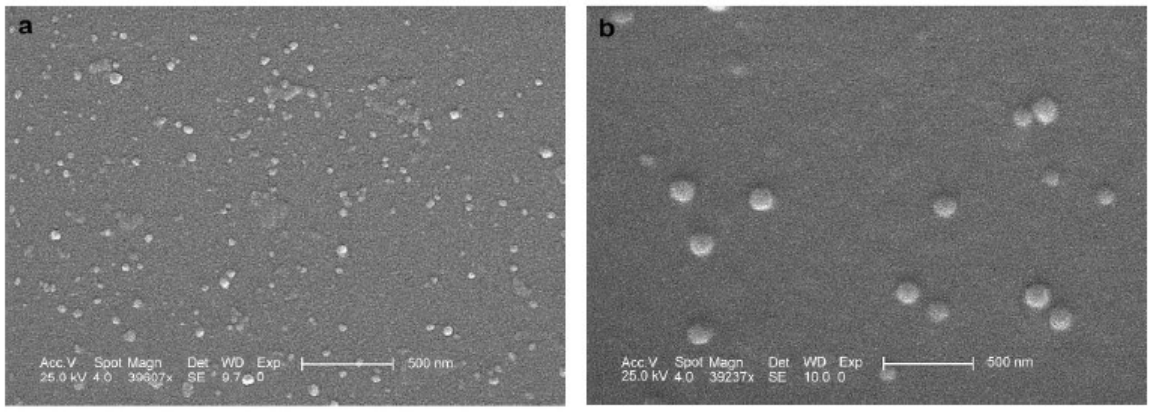

Figure 24 **ESEM photographs of (a) PML261 micelles and (b) CO–Hb conjugated PML261 micelles. [28]**

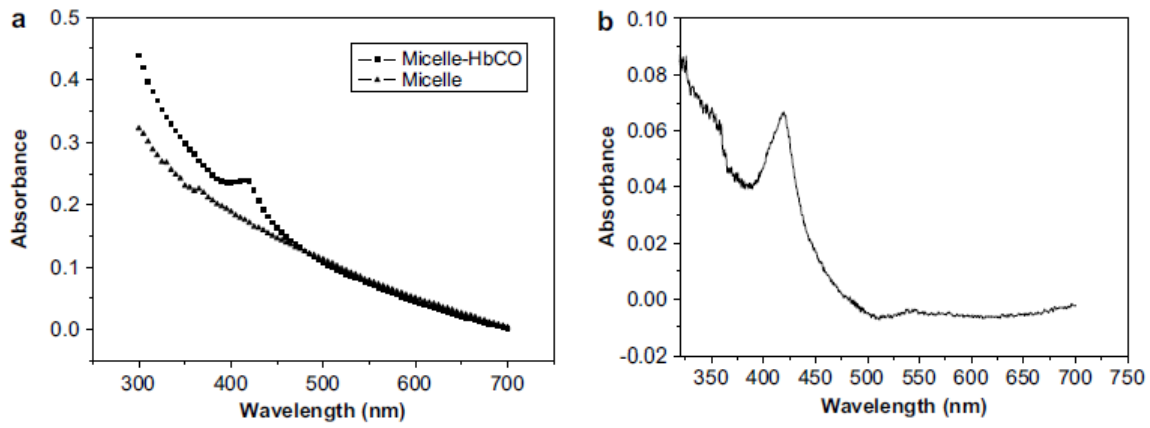

Figura 25 **(a) UV spectra of pure PML261 micelles and CO–Hb-conjugated PML261 micelles; (b) difference spectrum between the two spectra in (a). [28]**

Figure 26 shows the UV spectra of the HCM solution before and after O2 binding process. It is seen that after O2 gas was fed for 2h, typical absorbance peak of hemoglobin changed obviously from 419 nm to about 409 nm, indicating the state of hemoglobin was successfully transformed to O2-binding state. It implies that the Hb-conjugated micelles have oxygen carrying ability [28].

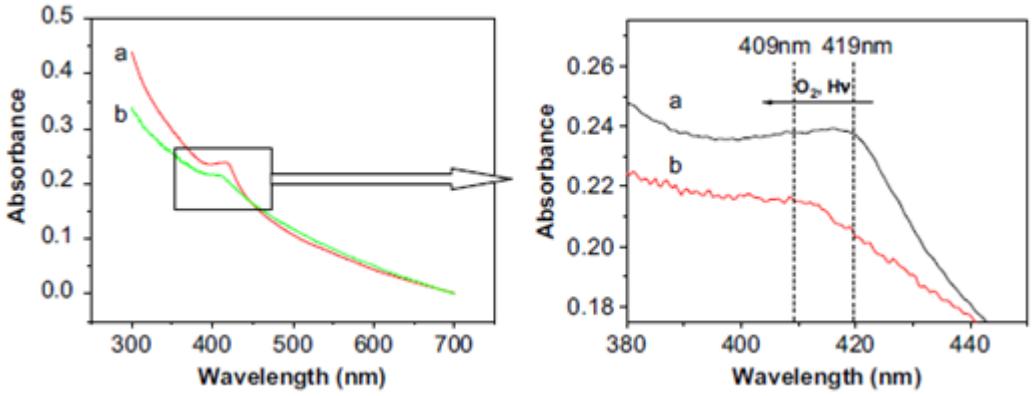

Figure 26 **UV spectra of HCM solution before (a) and after (b) O2 feeding for 2 h. [28]**

1.3. Aim of the work

To overcome the problem of tissues necrosis in the inner regions of 3D scaffolds with low porosity and static conditions due to the major consumption of nutrients respect to the diffusion, we decided to realize a new type of HBOC through chemical conjugation between bovine gelatine microbeads (75-150 μm diameter, 5% w/w cross-linked with glyceraldehyde-6-phosphate) and hemoglobin A_0 ferrous stabilized. The goal is to create a carrier of molecular oxygen as natural as possible without loss of Hb to insert inside 3D scaffolds or to utilize it as oxygen releasing biomaterial with which to build the scaffolds themselves.

The first question could regard the dimensions of the microbeads; we chose these dimensions because they are the most used in our research group, mostly for the construction of skin tissue.

Another observation could regard the possibility, after in vivo implantation and gelatine degradation, to get free Hb in the body with the risk of interaction with nitric oxide and subsequent vasoconstriction; however cells produces nonspecific proteases that degrade not only gelatin but Hb too; in fact, these Hbs undergo degradation before implantation, contemporary with gelatine.

At this point there could be the observation about the toxicity of the Fe(II) contained in heme groups and present in the scaffolds; Iron is an essential metal for almost all living organisms due to its involvement in a large number of iron-containing enzymes and proteins, yet it is also toxic. The potential of Fe(II) to catalyse hydroxyl radical formation via the Fenton reaction means that iron is potentially toxic. Its toxicity depends on the tissues in which Fe(II) is and on the concentration. [29]. However the quantity eventually used in a 3D scaffolds with our conjugated microbeads is very low. What are the risks in this case this concentration is not so low? It is fair to remember that iron is complexed with heme groups and not as free atoms in the body. Heme is a prosthetic co-factor so it is not degraded by proteases like the rest of Hb but it can be recycled to form new Hb molecules.

1.3.1. Approach to conjugation between microbeads (MBs) and hemoglobin (Hb)

Most reactions of protein modifications are completed in aqueous media. Thus crosslinking agent must be water soluble. Likewise, to reduce the denaturation of the protein during reaction, it is desirable that the cross-linking agent doesn't behave as a detergent or a chaotropic agent [30]. EDC and DSC cross-linking agent provide a spectrum of derivates activated for amino or hydroxyl groups coupling and can be useful in the cross-linking or modification of proteins such as hemoglobin. The stability of hemoglobin tetramers can be improved through cross-links among Hb monomers. This is easily obtained utilizing 1-ethyl-3-(3 dimethylaminopropyl)carbodiimide (EDC) chemistry, Zero-Length Cross-Linker class, due to the activation of the carboxylate groups of the side chains on the Hb surface. The activated ester intermediates react with primary amines of lysine residues on the surface of adjacent Hb molecules to form stable amide bonds. Even if the formation of EDC adducts with proteins can affect their net charge [42], conformation and enzymatic activity, it is a good method for activated coupling reactions and

cross-linking formation too [31]. Cross-linkers can bind the bioactive compound directly to the functionalized substrate (zero-length cross-linkers) or they can introduce a spacer of several Angstroms. A way to obtain activated surfaces, reactive to hydroxyl and primary amines groups, consists in introducing urethane function through DSC use [32, 33].

N,N`-Disuccinimidyl ester carbonate presents a carbonyl group containing two NHS ester and is highly reactive toward nucleophiles [34]. Utilizing these two chemistry strategies, we conjugated hemoblogin A_0 ferrous stabilized to gelatin microbeads used in tissue engineering as cell support. Before doing this, we performed several tests to characterize the microbeads surface to obtain an amino Molar Degree of Functionalization (ɳ) and to proceed with the conjugation. Successively we proceeded before with the conjugation and later with the evaluation of the capacity of Hb-microbeads to adsorb and release oxygen.

2. Materials and Methods

2.1. Materials

Bovine gelatine type B, Cottonseed oil, Span 85, Glyceraldehyde-6-phosphate, Human Hemoglobin A_0 Ferrous Stabilized, *N,N′*-Disuccinimidyl Carbonate (DSC) purum (≥95.0%), *N*-Hydroxysuccinimide 97% (NHS), *N*-(3-dimethylaminopropyl)-*N*`-ethylcarbodiimide bio extra (EDC), 5 Carboxy-X-rhodamine *N*-succinimidyl ester BioReagent (NHS-Rho, MW= 631.67 g/mol), dimethyl sulfoxyde (DMSO) were purchased from Sigma-Aldrich. Triethylamine (TEA, d=0,726 g/cm^3, MW= 101 g/mol), TriFluoroacetic Acid (TFA) LC grade, acetonitrile, acetone and water super purity solvent were purchased from Romil Pure Chemistry. Trypsin EDTA 200 mg/L was purchased from Lonza. DMEM low glucose (≤ 1000 mg) culture medium w/o Phenol-red was purchased from Gibco®. Albumine from Bovine Serum (BSA) was purchased from Sigma-Aldrich. OxyphorR2 was purchased from Oxygen Enterprises.

Reagent and solvent were used without further purification unless otherwise specified. Spectra/Por® Dialysis membranes MWCO:. 12-14,000 were purchased from Spectrum Laboratories, Inc.

2.2. Methods

2.2.1. Realization of gelatine microbeads (GMs)

2.2.1.1. Water in oil single emulsion

GMs were prepared using single emulsion method1. Briefly, six grams of gelatin (Type B, 225 Bloom Sigma Aldrich, St. Louis, MO) were dissolved in 20 ml of double-distilled water at 60°C. The gelatin solution was added drop wise to 40 ml of cottonseed oil pre-heated at 60°C forming water in oil emulsion by stirring. Subsequently, the emulsion was chilled at 5°C and gelatin microbeads were formed in the aqueous phase; then 60 ml of acetone precooled at 5°C was added. The resulting microbeads were filtered and

rinsed in acetone several times to remove the remaining oil on their surfaces. Finally the rinsed gelatin microbeads were dried under the hood overnight.

2.2.1.2. Crosslink of GMs

GMs were dispersed into an aqueous acetone solution containing Glyceraldehyde-6-phosphate (GAL, 20% w/w) and mixed for 24 h at 4°C to allow cross-linking. The cross-linked gelatin microbeads were filtered and rinsed with acetone to remove the residual crosslinking agent on their surfaces; afterwards they were sieved to obtain particles ranging from 75-150 μm.

2.2.2. Preliminary studies to determinate the average molar degree of functionalization (η) of free amine groups on the microbeads surface.

150 mg of GMs (75-150 μm diameter), previously dried under vacuum, were added to 4 mL of dry DMSO under argon flow. After 20 minutes large excess of TEA (9.1 μL, $6.57x10^{-5}$ moles) and the first addiction of NHS-Rho (35 mg, $6.57x10^{-5}$ mol) were added. The mixture was maintained under vigorous magnetic stirring for 1 hour and drying conditions at room temperature. Successively further quantities of NHS-Rho were added (15 mg, $2.81x10^{-5}$ moles) to the mixture under the same conditions for 2 hours. The microbeads were dialysed into Romil-SpS water for 72 hours utilising Spectra/por® dialysis membrane MWCO:.12-14000, successively precipitated in dialysis with phosphate buffer pH=7.4 for 12 hours. The final product was washed and centrifuged three times at 1500 rpm to completely remove absorbed rhodamine, lyophilized and stored at 4°C.

2.2.2.1. FTIR measurements in ATR mode

ATR experiments on gelatine microbeads and microbeads labelled with rhodamine were performed by using NICOLET 6700 Thermo Scientific

and considered in the region of spectra 4000-1000 cm^{-1}. Microbeads were were washed in water and dried under vacuum for 12 hours at room temperature.

2.2.2.2. Biological degradation

150 mg microbeads labelled with rhodamine were digested with 1 ml of Trypsin EDTA 200 mg/L under incubation for 24 hours at 37 °C.

2.2.2.3. HPLC characterization

HPLC experiments were performed by using Waters Alliance with Waters 2489 UV/Vis detector and NUCLEODUR® C18 Gravity 5 µm column (dimensions: 250 x 4.6 mm). Eluent solution was acetonitrile/water 9:1 in isocratic conditions with a flow of 0.7 ml/min, injection volume of 30.0 µL and run time of 30.0 minutes.

2.2.2.4. UV/Vis characterization

Spectrophotometric measurements were performed by VARIAN CARY 100 scan UV/Visible Spectrophotometer.

2.2.3. Human Hemoglobin-microbeads conjugation with two different coupling chemistries.

2.2.3.1. EDC chemistry (method A)

Synthesis of Hemoglobin-microbeads (HMsA): 100 mg of GMs (75-150 µm diameter) previously dried under vacuum were added to 2.5 mL of dry DMSO under argon flow and TEA (52 µL, $3.79x10^{-4}$ moles). The mixture was maintained under vigorous magnetic stirring for 5 minutes at room temperature. The human hemoglobin (6.44 mg, 9.47×10^{-5} moles) was dissolved in 0.5 mL of DMSO and EDC liquid (83 µL, $3.79x10^{-4}$moles) was added before completely dissolution. The solution containing hemoglobin and

EDC was added to microbeads solution. The reaction proceeded under vigorous magnetic stirring for 4 hours at room temperature.

Purification: HMsA were purified trough washing and centrifuged at 400 rpm than dialysed into DMSO for 24 hours utilising Spectra/por® dialysis membrane MWCO:.12-14000. After precipitation the microbeads were lyophilized and stored at -20 °C.

2.2.3.2. DSC chemistry (method B)

Synthesis of NHS-microbeads: 100 mg of GMs were added to DSC powder and dried under argon flow for 30 minutes. DSC powder (82.00 mg, $3.8x10^{-4}$ moles) was dissolved into 2.5 mL of dry DMSO with the microbeads (75-150 μm diameter) above and let under magnetic stirring for 10 minutes; after this time, TEA (53 μL, $3.8x10^{-4}$moles) was added to the solution. The reaction proceeded for 2 hours in dry conditions at room temperature.

Purification: NHS-microbeads were purified trough washing and centrifugation at 1400 rpm. After precipitation, microbeads were lyophilized and stored at -20 °C.

Synthesis of Hemoglobin-microbeads (HMsB): 100 mg dried NHS-microbeads were added to human hemoglobin (6.46 mg, $9.48x10^{-5}$moles) and let under argon flow for 30 minutes. Then 0.5 mL of DMSO and TEA (53 μL, $3.8x10^{-4}$moles) were added to the powder mixture. The reaction proceeded under vigorous magnetic stirring for 4 hours at room temperature.

Purification: HMsB were purified trough washing and centrifugation at 400 rpm and then dialysed into DMSO for 24 hours utilising Spectra/por® dialysis membrane MWCO:.12-14000. After precipitation, microbeads were lyophilized and stored at -20 °C.

2.2.3.3. FTIR measurements in ATR mode

ATR experiments on HMsA and HMsB were performed by using NICOLET 6700 Thermo Scientific and considered in the region of spectra

4000-1000 cm^{-1}. Microbeads were were washed in water and dried under vacuum for 12 hours at room temperature.

2.2.3.4. Microstructural analysis

The microstructures of HMsA and HMsB were investigated by scanning electron microscope (SEM). In particular, the microbeads were mounted onto metal stubs using double sided adhesive tape and then gold-coated using a sputter coater at 15 mA for 20 min [35].

2.2.3.5. Analytical determination of Fe(II)

Experiments were performed using ICP-MS by Varian to determine the quantity in mg/L of Fe(II) in the digested solutions of HMsA and HMsB.

2.2.4. Phosphorescence Quenching Microscopy (PQM)

2.2.4.1. Technique

Phosphorescence Quenching Microscopy (PQM) is an optical technique whose spatial and temporal resolutions depend on the experimental set up. The basic principle is that it is possible to correlate oxygen concentration to the decay time of a phosphorescent probe. Phosphorescence intensity of a probe can be decreased by a wide variety of processes: such intensity decrease is named quenching. Collisional quenching, in particular, occurs when the excited state phosphor is deactivated upon contact with some other molecules in solution, the quenchers. These collisions determine a decrease in the emission lifetime. It is possible to relate the characteristic phosphorescence lifetime of a probe to the concentration of a quencher dissolved in the solution. In this case the quencher is oxygen and the phosphorescent probe is a Pd-meso-tetra (4-carboxyphenyl) Porphyrin dendrimer, OxyphorR2 (Oxygen Enterprises). The collision between a triplet state solute molecule and molecular oxygen has a high probability to generate an energy transfer between molecules. After collision, the excited molecule is

returned to the ground state without light emission. Therefore the total emitted phosphorescence is decreased while the decay rate of triplet state increases, i.e. phosphorescence lifetime decreases, according to Stern-Volmer equation:

$$1/\tau=1/\tau_0 +K_Q pO_2$$

where:

- τ is the decay time measured;
- τ_0 is the decay time in absence of oxygen;
- K_Q is the quenching constant, depending on the oxygen solubility in the calibration material.

[35, 36].

This technique is characterized by: non-invasiveness and high spatial and temporal resolution. In this study PQM technique is used to measure and evaluate oxygen release and absorption kinetics by haemoglobins conjugated to microbeads.

2.2.4.2. Instrumentation

PQM (general scheme in figure 2) was assembled in our laboratories utilizing an inversion microscope (Olympus IX-70), xenon flash lamp (ORIEL Series Q Convective Lamp Housing, model 6427) as light source, interference dichroic filters (510-550 nm and >590 nm) from Olympus, a photomultiplier (PMT, Hamamatsu R6357) and an oscilloscope (Tektronix TDS 224). The microscope is the core of PQM instrumentation. The xenon lamp emits light passing through the interference filter (510-550 nm) to be reflected on the phosphorescent probe. The phosphorescence emission passes through the second interference filter (>590 nm) before being captured by the photomultiplier. The amplified electrical signal is read by the oscilloscope and the decay lifetime is calculated from the best fit to the single exponential

decay curve through Matlab®. Then the decay lifetime measured is converted in O_2 partial pressure.

In our case, the phosphorescent probe is a Pd-meso-tetra(4-carboxyphenyl)Porphyrin dendrimer (Oxyphor R2) with a concentration of 90 µM. Data analysis was carried out with Matlab software. [GUA]

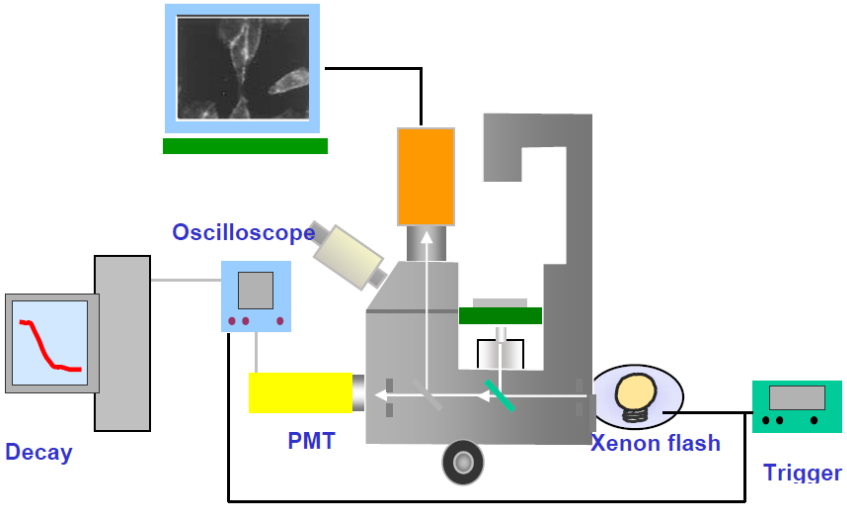

Figure 27 **Scheme of PQM instrumentation. [35]**

2.2.4.3. Measurements

Three Pyrex containers, 8 ml capability, were realized for our experiments. They have a side opening to put functionalized microbeads inside and for N2 input in the case of oxygen release measurements. Side opening was realized to able the microscope light to pass from the top to the bottom of the containers. DMEM low Glucose culture medium was enriched with Oxyphor R2 90 µmol (0.25 mg/ml) and BSA 1% w/w, sterilized with a 0.22 µm filter and put inside containers previously sterilized in the quantity of 8ml per each one.

Two types of experiments were performed: Adsorption and Releasing of molecular oxygen.

2.2.4.3.1. Oxygen adsorption

8 ml culture medium was out in the container with 0.21 atm O2 (air saturation). Microbeads, sterilized in ethanol solution (90%), were put inside after treatment in organic solvent (DMSO) and blowing with N2 to remove Oxygen. From this moment onwards, measurements at 0, 1, 2, 3, 21 and 24 hours were performed with PQM to observe the absorption of oxygen by microbeads.

Four conditions were examined and three containers for each one were used to have more accurate measures and a standard deviation: Culture Medium only, Culture Medium with GMs, Culture Medium with HMsA and Culture Medium with HMsB.

2.2.4.3.2. Oxygen release

After analyzing absorption measurements, O2 release measurements were performed. In this case N2 was blown in sterilized (0.22 μm filtered) culture medium to get O_2 out of the container. Microbeads were put inside during an opening of 10 seconds. The same thing was done for Medium only to have the same exchange of gas with the external environment. In these cases we performed the same number of measurements but in different conditions: Culture Medium only, Culture Medium with GMs (water treatment), Culture Medium with GMs (organic solvent treatment), Culture Medium with HMsA (water treatment), Culture Medium with HMsA (organic solvent treatment), Culture Medium with HMsB (water treatment) and Culture Medium with HMsB (organic solvent treatment).

All the reactions were done in organic solvent (DMSO); conditioning in DMSO was made to remove oxygen from Hb and microbeads (organic solvents have low solubility for O_2); washing in H_2O was made to saturate Hb of O_2.

3. Results and discussion

3.1. Functional modification of GMs surface

First of all, a calibration curve was derived from spectrophotometric measurements of free rhodamine in an aqueous solution to correlate absorption and concentration. Rhodamine used for this study has a wavelength of absorption (λ_{ex}) at 575 nm and a wavelength of emission (λ_{em}) at 600 nm.

GMs functionalization was performed in two steps. First, GMs were rhodaminated by conjugation with 5Carboxy-X-rhodamine *N*-succinimidyl ester to obtain GMs-Rho microbeads.

GMs-Rho microbeads were characterized by FTIR with ATR mode experiments on gelatine microbeads and microbeads labelled with rhodamine were performed by using NICOLET 6700 Thermo Scientific and considered in the region of spectra 4000-1000 cm-1. Gelatine microbeads showed characteristic picks at 1653.0 (amide I) and 1544.7 (amide II) cm-1 attributed to the amide groups, typical of peptide bond of proteins. The microbeads labelled with rhodamine showed also one pick at 3080 cm-1, characteristic of the aromatic C-H stretch of the rhodamine.

The resulting rhodaminated microbeads were digested by trypsin to obtain a homogeneous solution of small protein fragments. The degree of superficial functionalization (ɳ) was estimated by HPLC and UV/Vis methods. Several examples useful to estimate the modification degree of amino groups on the surface of gelatine microbeads are reported in literature. In particular, it is reported the conjugation of the aminated gelatine with 2,3-dihydroxybenzoic acid and the estimation of functional modification degree through UV spectrophotometer [37]. The method used in this study consists in the estimation of surface amino groups through saturation method using 5 Carboxy-X-rhodamine *N*-succinimidyl ester (NHS-Rho). Reaction was performed in DMSO solvent to avoid GMs swelling and consequent free

rhodamine adsorption. The purification through dialysis in DMSO is an important step because it allows to remove the excess rhodamine. The degradation of 50 mg of GMs-Rho led to the formation of various fragments: simple peptides, rhodaminated peptides and free rhodamine. The stoichiometric ratio existing between bound rhodamine and amino groups is 1:1 because one molecule of the dye used is able to bind just one amino group on the surface of GMs. The knowledge of the stoichiometric ratio is very important because it makes possible to evaluate the quantity of free amino groups on the surface considering chromatographic and spectrophotometric methods that represent an easy procedure for the estimation of η, expressed in terms of mol/mg, mol of free amino groups on 1 mg of GMs. We chose HPLC as chromatographic method for its reliability, reproducibility and sensibility. First, we made a calibration curve of the HPLC with rhodamine (Fig. 28): a mother solution was prepared dissolving 1.6 mg of rhodamine in 1 ml of water SpS and six samples were obtained through dilution with a final volume of 1 ml. The curve was obtained measuring the average percentage areas (%A) of the picks, concerning 20 µl of injection volume in triplicate for each sample, and correlating them to the number of mol of the samples, according to the method of external standardization.

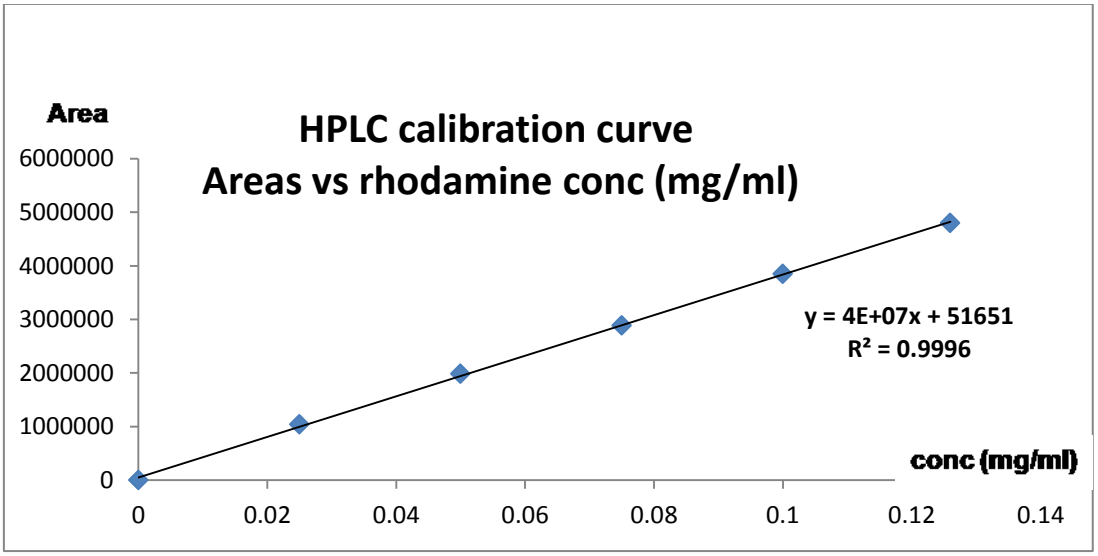

Figure 28 **UV/Vis Spectrophotometer calibration curve for rhodamine (Abs vs moles of rhodamine)**

Elutions were performed in isocratic conditions with a blend of 10% water SpS (containing 1% TFA) and 90% acetonitrile (containing 1%TFA) with a flow of 0.7 ml/min at room temperature. Absorption peaks were collected at a wavelength of λ=550 nm, close to the absorption wavelength of rhodamine that is 575 nm. Within the molar range of $4.7x10^{-8}$ – $2.4x10^{-7}$, the six %A of rhodamine presented good linear relation with the number of moles (R^2=0.9996). After doing the calibration curve, we proceeded with the separation of the mixture of simple peptides, rhodaminated peptides and free rhodamine through elution in the same conditions above.

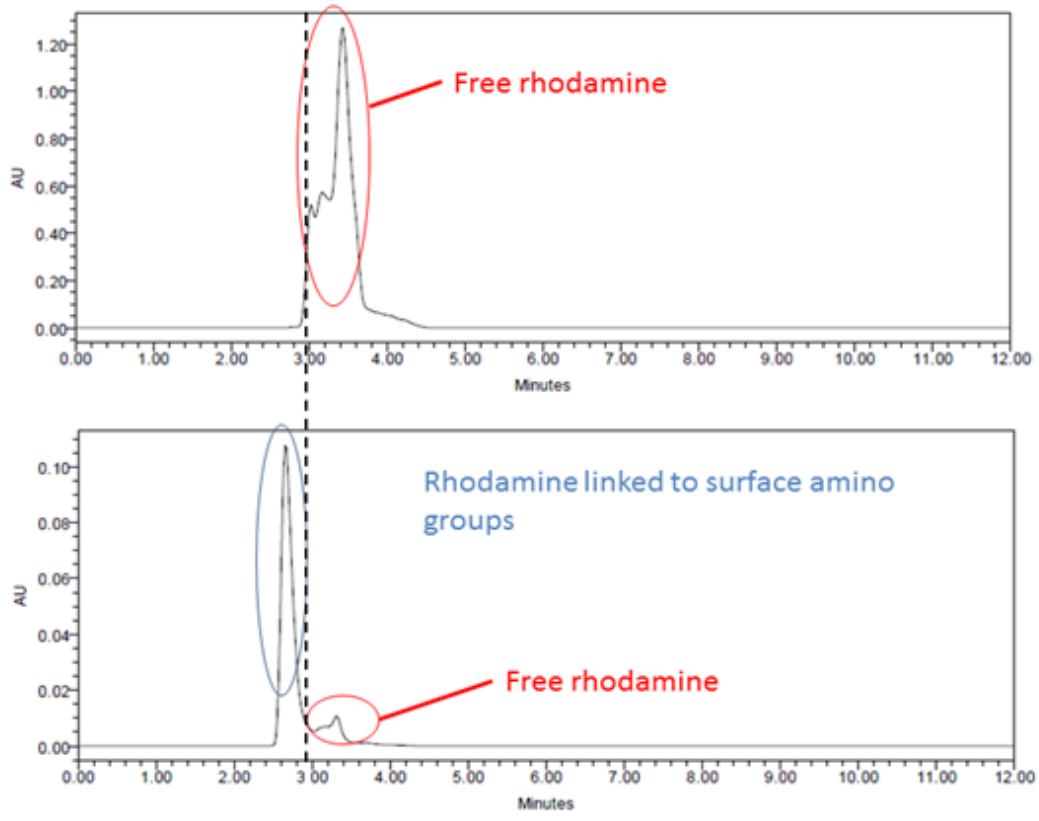

Figure 29 **HPLC chromatograms of free rhodamine (a) (500_M) and rhodamine-peptide plus free rhodamine (b) (500_M). Retention times: (a) TRa = 3.31±7.6x10-3 min (b) TRb = 2.66±6.7x10-3 min.**

In figure 29 two different elution profiles are shown: the free rhodamine (a) and the mixture composed of GMs-rhodamine fragments and free rhodamine (b). It's clearly shown that they have different times of retention (t_R): $3.31 \pm 7.6 \times 10^{-3}$ min for free rhodamine and $2.66 \pm 6.7 \times 10^{-3}$ min for rhodaminated fragments so that we could discriminate the two species. Once we had found the different t_R of the species, an exactly weighed amount of rhodaminated microbeads (50 mg) was treated with 300 μL of Trypsin EDTA 200 mg/L solution in 700 μL water until complete degradation at 37°C for 24 hours. An aliquot of the resulting solution was diluted until a concentration of 3 mg per 1 ml and 3 injections (L, L1 and L2) of 20 μl, corresponding to 0.06 mg of GMs-rhodamine, were done. The three chromatographic profiles are shown in figure 30. The average %A of the peaks regarding GMs-rhodamine fragments was calculated and the corresponding value of mol was observed on the calibration curve. Considering that the stoichiometric ratio between rhodamine and free amino groups on the surface of GMs is 1:1 and the injection quantity of GMs-rhodamine is 0.06 mg, corresponding to 5.10×10^{-8} moles of rhodaminated fragments or, as assumed above, of surface amino groups. So we have 8.50×10^{-7}mol of surface amino groups per 1 mg of gelatin microbeads (5% cross-link) with diameters 75-150 μm. This value is the degree of superficial functionalization (η_s).

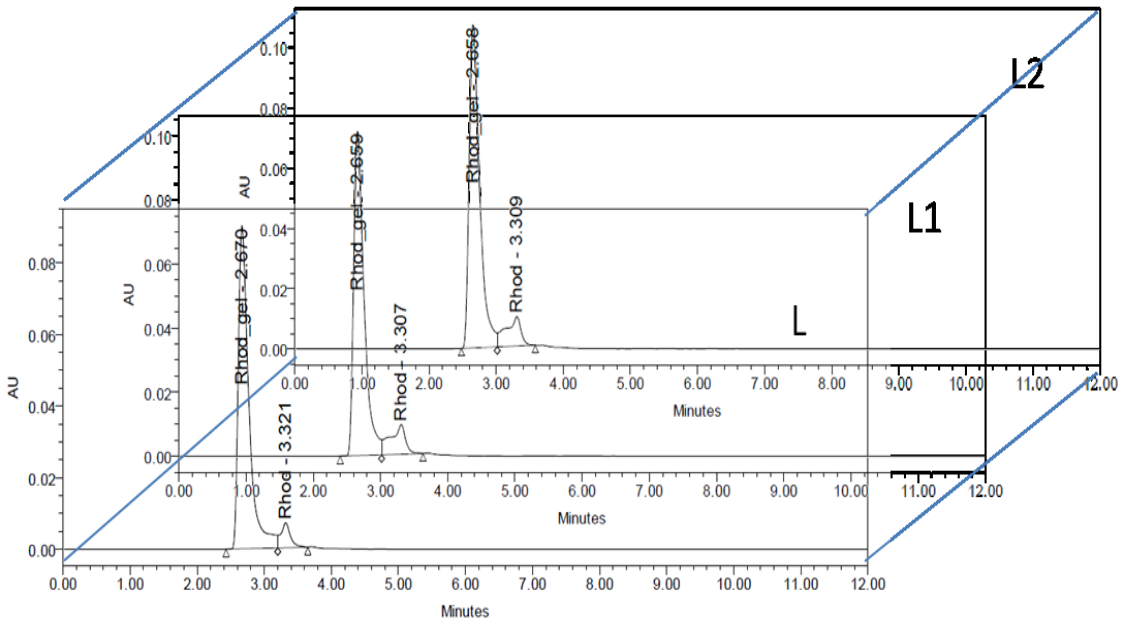

Figure 30 **HPLC chromatograms of samples L, L1 and L2. Retention times: TR1(rhodamine)=3.31±7.6x10-3 min, TR2(rhod-gel)=2.66±6.7x10-3 min**

To be sure that the calculated value of ɳ is right, we decided to use spectrophotometric UV/Vis technique too combined with HPLC. The same samples used for the calibration curve of HPLC with rhodamine were used for that one of spectrophotometer. Within the molar range of $2.5x10^{-8}$ - $2.0x10^{-7}$, the six values of absorbance at 550 nm (the same wavelength of HPLC UV/Vis detector) of rhodamine presented good linear relation with the number of mol (R^2=0.9972).

The same mixture of fragments used for HPLC measurements was used for spectrophotometric measurements too. Its original concentration (50 mg/ml) was diluted until obtaining three samples of 1ml per each one (L, L1 and L2) with a concentration of 0.167 mg/ml. After doing this, total absorbance, regarding free rhodamine and GMs-rhodamine fragments, was collected for each sample and the average absorption was correlated through the calibration curve. The molar quantity of total rhodamine for 0.166 mg of GMs-rhodamine resulted $1.37x10^{-7}$mol that corresponds to a value of

$8.25x10^{-7}$ moles (M1) for 1 mg of GMs-rhodamine. Concerning HPLC chromatograms at 550 nm, the molar quantity of free rhodamine is $2.01x10^{-8}$ moles (M2) for 1 mg of treated GMs-rhodamine The difference between M1 and M2 is $8.05x10^{-7}$ mol per 1 mg of gelatin microbeads (5% cross-link) with diameters 75-150 μm. This value is very closed to that one found through HPLC. As said before, this was just to be sure that the evaluation of η with HPLC was well-done; in fact, we chose to use η found trough HPLC because it highlights two different species with two different retention times.

3.2. Hemoglobin conjugation to gelatin microbeads: EDC and DSC strategies

Functionalization of smooth microbeads has characterized by two fundamental and interconnected aspects. The first one regards the superficial distribution of chemical reactive groups to bind the right stoichiometric quantity of functional molecules; the second important aspect is the cost.

EDC and DSC cross-linking agent provide a spectrum of derivates activated for amino or hydroxyl groups coupling and can be useful in the cross-linking or modification of proteins such as hemoglobin. The stability of hemoglobin tetramers can be improved through cross-links among Hb monomers. This is easily obtained utilizing 1-ethyl-3-(3 dimethylaminopropyl)carbodiimide (EDC) chemistry, Zero-Length Cross-Linker class, due to the activation of the carboxylate groups of the side chains on the Hb surface. The activated ester intermediates react with primary amines of lysine residues on the surface of adjacent Hb molecules to form stable amide bonds (Fig. 31). Even if the formation of EDC adducts with proteins can affect their net charge, conformation and enzymatic activity [42], it is a good method for activated coupling reactions and cross-linking formation too [31].

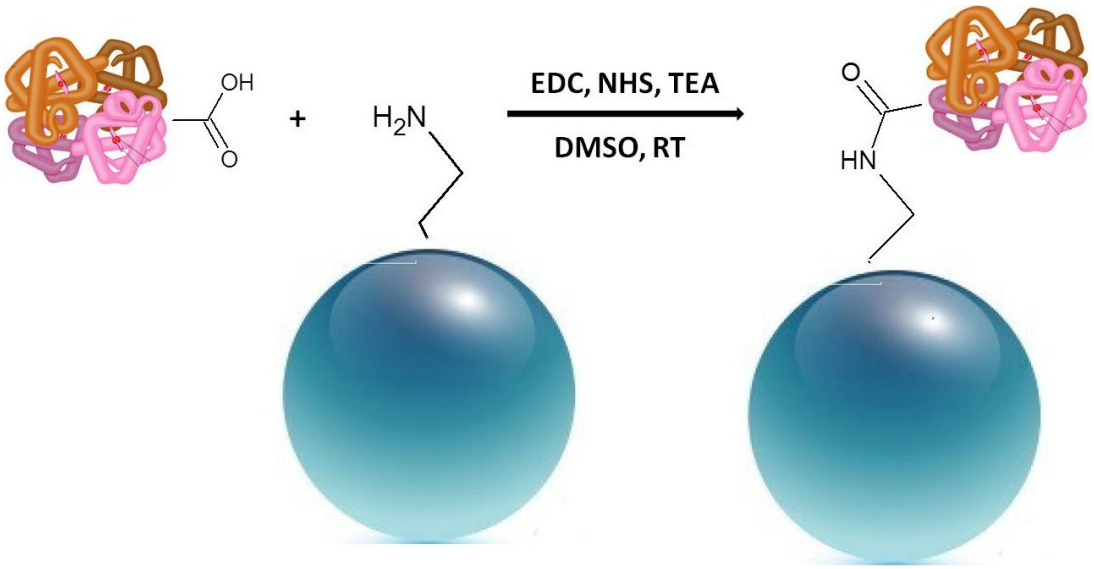

Figure 31 **EDC reaction mechanism.**

Cross-linkers can bind the bioactive compound directly to the functionalized substrate (zero-length cross-linkers) [39, 40, 41] or they can introduce a spacer of several Angstroms. A way to obtain activated surfaces, reactive to hydroxyl and primary amines groups, consists in introducing urethane function through DSC use [32, 33].

N,N`-Disuccinimidyl ester carbonate presents a carbonyl group containing two NHS ester and is highly reactive toward nucleophiles [34] (Fig. 32).

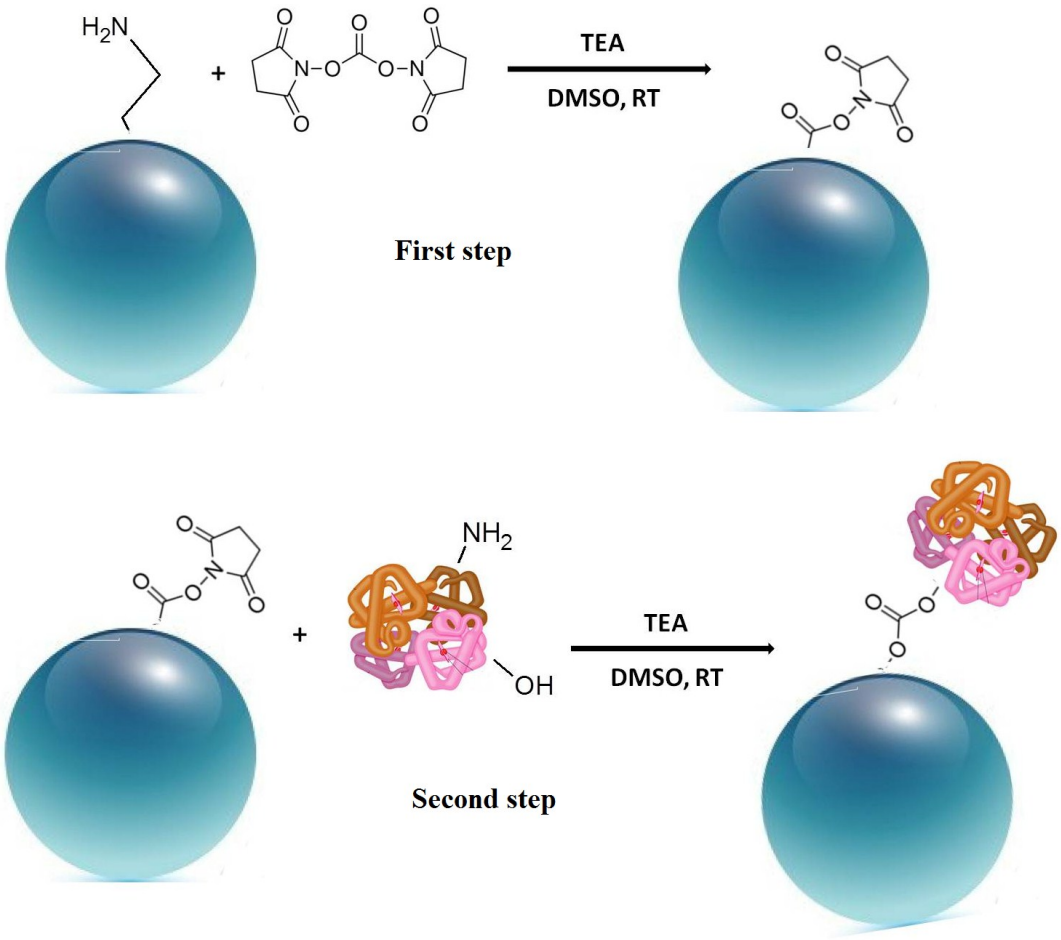

Figure 32 **DSC reaction mechanism.**

EDC/NHS chemistry stabilizes Hb through crosslinking among subunits [26, 37, 38] but there is a negative aspect too: it produces not only microbeads conjugated to Hb but aggregates of Hb and/or microbeads conjugated to these aggregates too. This may lead to steric hindrance for inner molecules of Hb with the consequence of no oxygen absorption and release for these molecules due to the impossibility to change their conformation.

DSC chemistry [32, 33] avoids the formation of aggregates letting Hb free to bind and release oxygen. This chemistry is an easy approach to bind Hb to GMs surfaces. In this case the negative aspect is the absence of cross-link among subunits. So it was decided to evaluate which is the best chemistry through oxygen absorption and release measurements.

Coupling reaction is influenced by Hb volume. Oxygen absorption and release are closely dependent on the reaction stoichiometry that depends not only on the microbeads surface but on the volume of the protein (Hb) too. In fact, oxygen absorption and release measurements showed the same results for the stoichiometric quantity of Hb and 1/6 of it used in two different reactions so we decided to use a less quantity of Hb respect to that stabilized by stoichiometric ratios.

After doing reaction, microbeads were washed in water and dried under vacuum for 12 hours at room temperature. 5 mg of Hb, gelatine microbeads, A and B microbeads were weighted and utilized for the ATR measurements considering the spectra in the 4000-400 cm^{-1} region. The ATR spectra of hemoglobin, gelatine microbeads and Hemoglobin-gelatine microbeads coupled through A and B methods showed the pick at 1652.9, 1652.0, 1645.1 and 1644.8 cm^{-1} respectively, which are characteristic for the amide I vibration. Around pick at 1654.0 cm^{-1} corresponding mainly to a α-helix structure content due to C=O stretching vibration and N-H bending mode [38]. The intensities ratio of hemoglobin microbeads coupled A and B and gelatine microbeads considered for picks of the amide I (table Z), showed that the portion of α-helix characteristic of hemoglobin structure are 1.26:1 and 1.36:1 respectively. The intensity ratio of hemoglobin and gelatine microbeads was of 1.42:1. The relationship between the intensities ratio allowed us to establish that 5 mg of HMsA and HMsB respectively contain a portion of hemoglobin, which are in agreement with the oxygen release assays. Furthermore the ATR spectra showed absorption peaks in the region 400 cm^{-1} until 650 cm^{-1} characteristics of C=O stretching of the heme group complexed with Fe (II) in the Hb, microbeads A and B. In figure 33 the peaks of some experiments are shown.

Tabel 1 Table Z: ATR picks and intensity

	Pick (cm^{-1}) C=O bending N-H stretching	Band Intensity	Band Intensity ratio
Gelatine microbeads	**1652.0**	**61960**	**1**
Hemoglobin	**1652.9**	**88129**	**1.42**
Microbeads A	**1645.1**	**78146**	**1.26**
Microbeads B	**1644.8**	**83906**	**1.36**

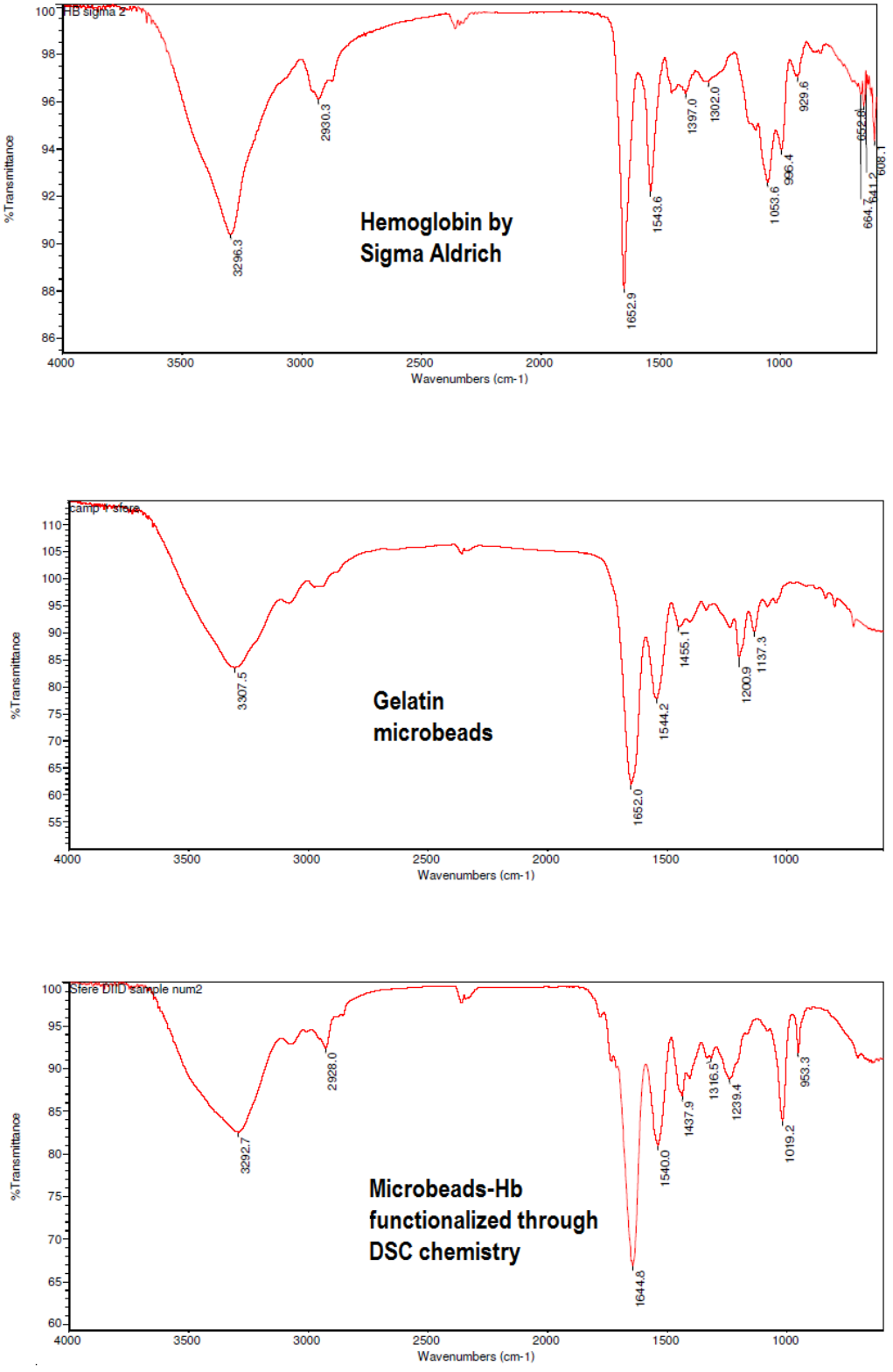

Figure 33 **ATR peaks for Hb by Sigma, non-functionalized microbeads and HMsB.**

ICP-MS (Varian) measurements (ICP) showed a concentration for Fe(II) of 1.287 mg/L HMsA and of 1.473mg/L for HMsb.

Microstructural analysis by SEM showed differences among non-functionalized microbeads, HMsA and HMsB surfaces. As shown in figure 34 GMs are the most corrugated and HMsB are the most velvety. HMsA are in the middle. These observations could be explained with a more efficiency of DSC chemistry respect to DSC one, supposing the velvety layer is composed by Hb molecules.

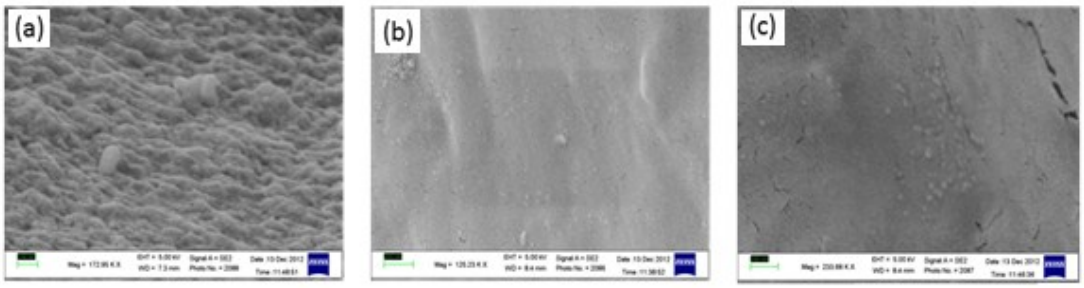

Figure 34 SEM images of non-functionalized microbeads (a), HMsB (b) and HMsA (c).

3.3. PQM measurements

3.3.1. Oxygen Adsorption

Measurements analysis showed a slight decrease of O_2 concentration for culture medium only (Figure 35, 36 and 37). DMEM low glucose w/o phenol-red is enriched with proteins; besides, BSA is put inside to stabilize Oxyphor R2. Proteins are subject to oxidation and this is the reason why we measured a slight decrease of O_2. To be sure about this, we performed the same measurements in water and no decreases were observed.

In the case of non-conjugated microbeads (GMs) there is a greater decrease of O_2 respect to culture medium only. To understand why it happens we performed measurements through ‘’Presence Oxy-4 mini’’ instrument to have a continuous monitoring of oxygen consumption in water containing gelatin powder and in water containing gelatin microbeads. In the first case

there was no oxygen decrease in 24 hours but a decrease was observed in the second one. This is the demonstration that there is an oxygen absorption by microbeads.

Microbeads-Hb showed a greater decrease respect to decreases previously described.

Two kinds of chemistries were utilized to realize functionalized microbeads: EDC and DSC.

EDC chemistry is a one-step reaction and requires all the reagents at the same moment. This leads to the formation microbeads-HB, but Hb-Hb too with possible steric hindrance of some Hb molecule. DSC chemistry is a two-steps chemistry that requires amino-functionalization of microbeads before and conjugation with hemoglobin in a second moment. As it can be supposed, DSC chemistry permits a better conjugation with the hemoglobin in solution avoiding the formation of Hb-Hb only or aggregates with the consequence of steric hindrance. In fact, as shown in fig. 37, both chemistries presented very good results but HMsB shows better O_2 adsorption respect to HMsA.

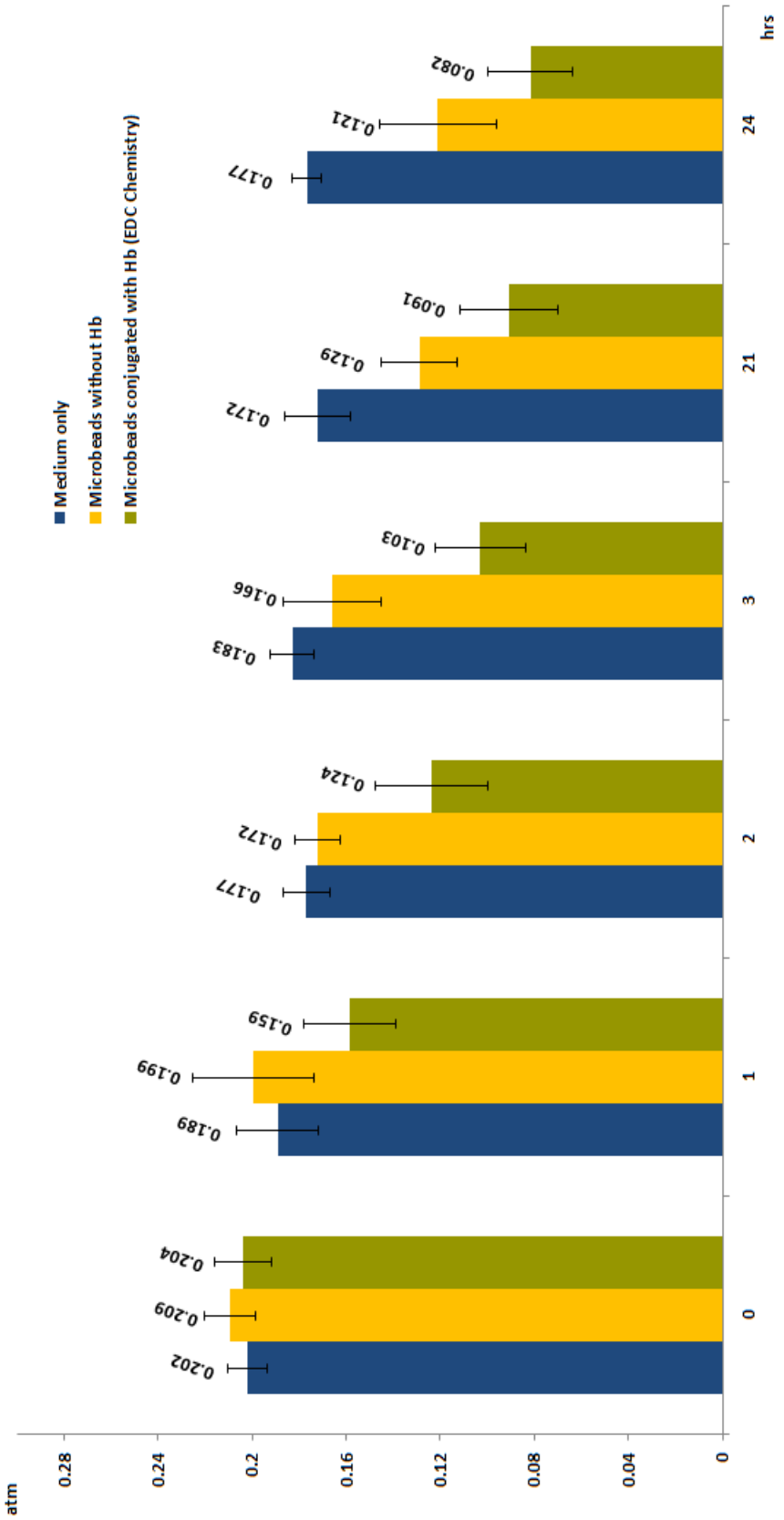

Figure 35 **Oxygen adsorption measurements – data elaboration (pO2 vs time)**

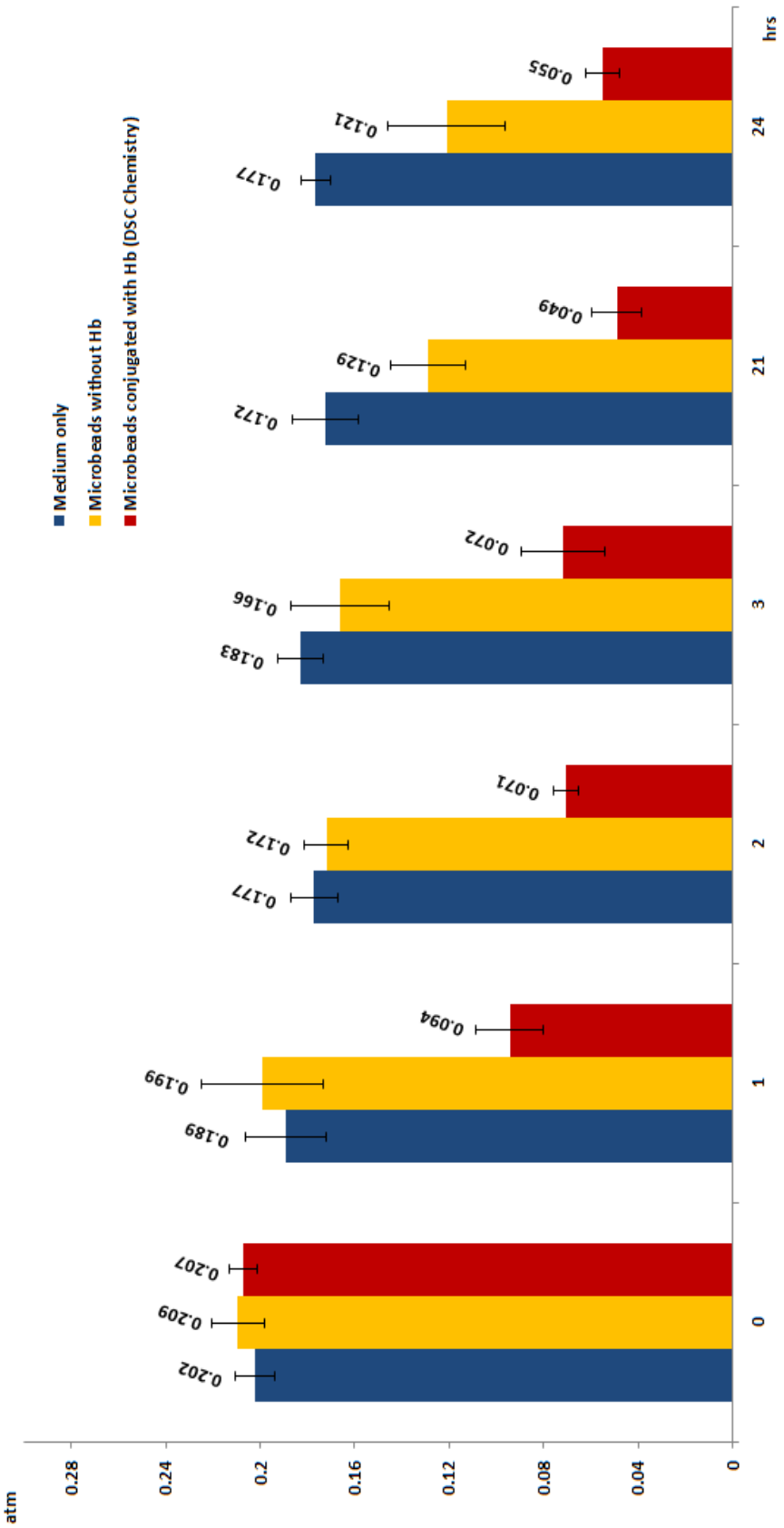

Figure 36 **Oxygen adsorption measurements – data elaboration (pO2 vs time)**

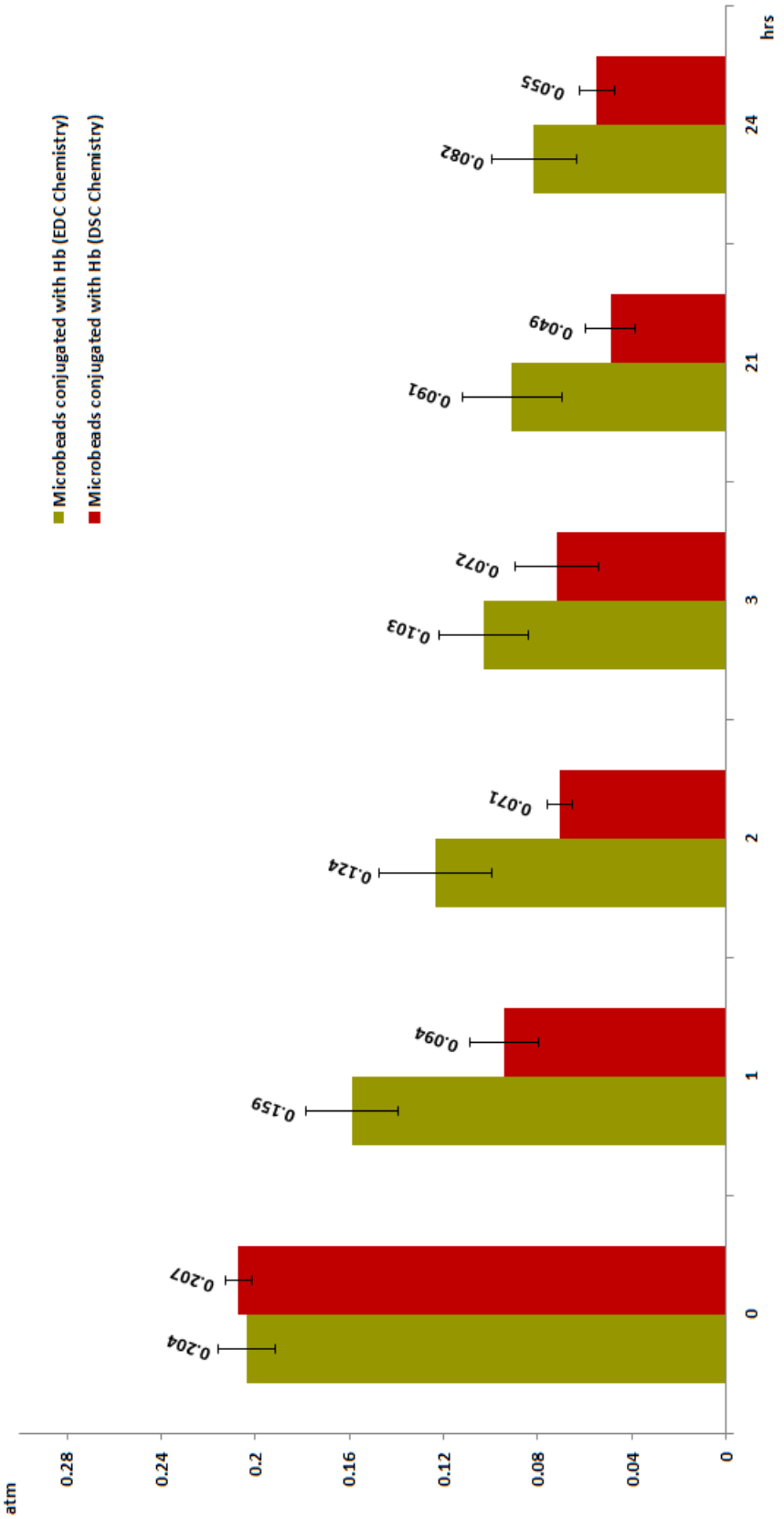

Figure 37 **Oxygen adsorption measurements – data elaboration (pO2 vs time)**
Comparison between HMsA and HMsB oxygen adsorption

3.3.2. Oxygen release

Medium only experiments showed a slight increase of O2 due to the 10 seconds opening of the container. In fact, as said before, containers with medium only were opened for the same time of the other ones to simulate similar conditions. So this increase is due to the input of air inside the container.

Non-functionalized microbeads measurements showed almost the same increase of medium only ones, as expected, due to the absence of Hb loaded with O_2. The increase is just a few quantities bigger than that with medium only because, as seen in adsorption measurements, microbeads are able to capture oxygen. There is a slight difference between GMs washed in water and GMs washed in DMSO but the difference is not relevant and depends on the O_2 content absorbed by water that has more O_2 of organic solvents.

HMsA and HMsB washed with organic solvent showed a very low release of oxygen; DMSO is an organic solvent with a low solubility for oxygen and the results showed that it got out a big percentage of O_2 from Hb.

HMsA washed in water showed a sensible increase in oxygen concentration in the medium, demonstrating that Hb was rich of oxygen and was able to release it.

HMsB washed in water is the last condition we analyzed. The release is almost the same of that one concerning HMsA washed in water, but it presents a different kinetic of release, with low values at the beginning and high values at the end of measurements. Besides, O_2 release is better in values respect to the condition without linker. These kinetics are the best ones for our goal because cells take oxygen from medium and they need supplementary oxygen after first hours and not immediately.

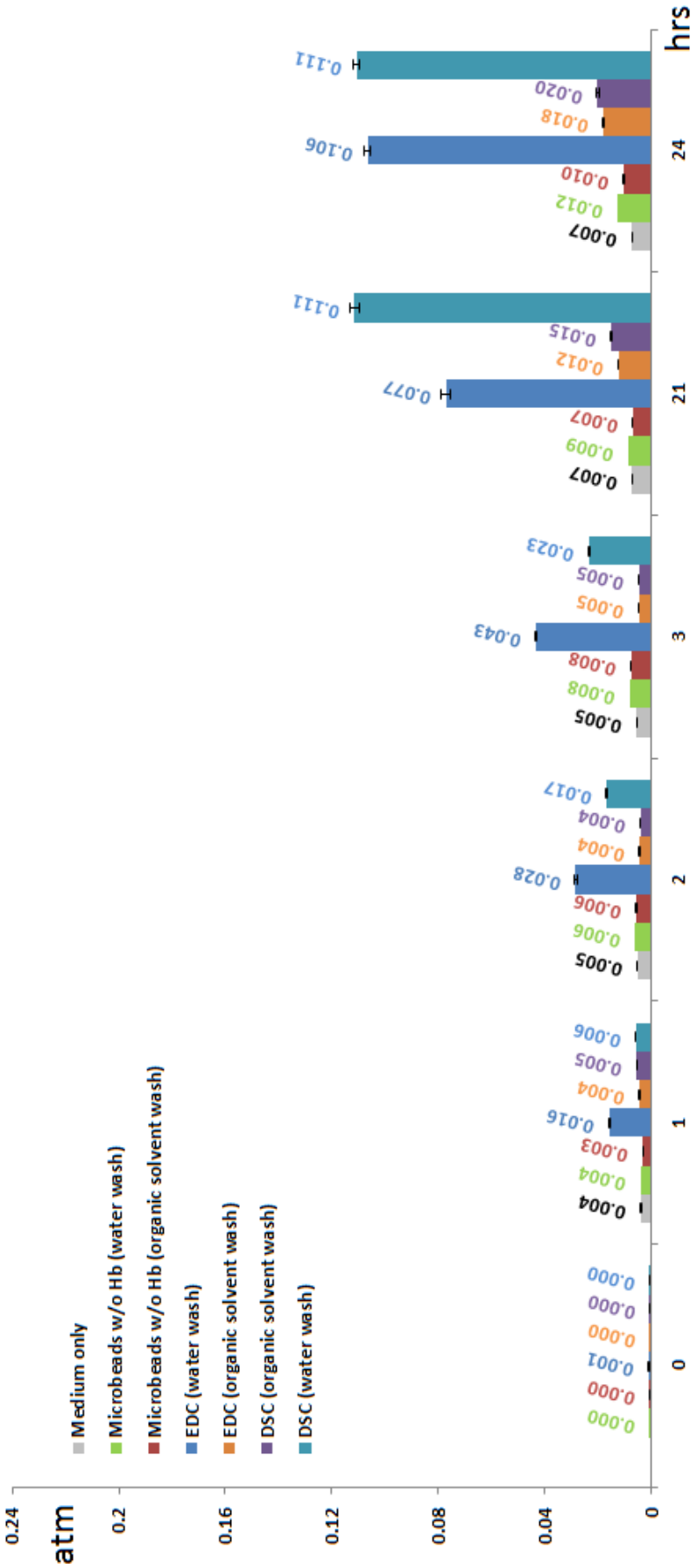

Figure 38 **Oxygen adsorption measurements – data elaboration (pO2 vs time)**

4. Conclusions and future developments

Hemoglobin-based oxygen carriers (HBOCs) have been developed in last years as an alternative to red blood cells (RBCs) mostly composed of Hemoglobin (Hb) that is the natural carrier for oxygen transport in mammals.

To overcome the problem of tissues necrosis in the inner regions of 3D scaffolds with low porosity and static conditions due to the major consumption of nutrients respect to the diffusion, we decided to realize a new type of HBOC through chemical conjugation between bovine gelatine non-porous microbeads (75-150 μm diameter, 5% w/w cross-linked with glyceraldehyde-6-phosphate) and hemoglobin A_0 ferrous stabilized. The goal is to create a carrier of molecular oxygen as natural as possible without loss of Hb to insert inside 3D scaffolds or to utilize it as oxygen releasing biomaterial with which to build the scaffolds themselves. Tissue engineering has always characterized by the death of the cells in the inner parts of the scaffolds due to the major consumption of nutrients respect to the diffusion. In the other cases, diffusion causes a wash out of extracellular matrix as an undesirable effect. As known, oxygen is the fundamental nutrient for the cells and we realized a new type of HBOC trough EDC/NHS and N,N′-Disuccinimidyl Carbonate (DSC) chemistries. We made several PQM test to evaluate if the HMsB (conjugated microbeads through DSC reaction) have better performance of HMsA (conjugated microbeads through EDC/NHS reaction) and we evaluated molecular oxygen absorption and release. Until now, no studies are published about the surface characterization and Hb-functionalization of non-porous-gelatin microbeads. In fact, we first characterized the surface of gelatin microbeads and then, after calculating the average amino Molar Degree of superficial functionalization (η), we conjugated hemoglobin to the surface of the microbeads and performed experiments to observe Hb presence and how it works. We observed that our HBOC release oxygen in hypoxic conditions and adsorb oxygen in O2 saturation conditions. Besides, DSC

chemistry resulted more efficient than EDC/NHS one and HMsB have better performances than HMsA.

References

1) Ivan Martin, David Wendt, Michael Heberer. The role of bioreactors in tissue engineering. *Trends in biotechnology*, Volume 22, Issue 2, February **2004**, 80–86.

2) Lewis MC, MacArthur BD, Malda J, Petter G, Please CP. Heterogeneous proliferation within engineered cartilaginous tissue: the role of oxygen tension. *Biotechnol Bioeng* **2005**; 91(5):607-15.

3) Malda J, Klein TJ, Upton Z. The roles of hypoxia in the in vitro engineering of tissues. *Tissue Eng.* **2007** Sep;13(9):2153-62.

4) Obradovic B, Carrier RL, Vunjak-Novakovic G, Freed LE. Gas exchange is essential for bioreactor cultivation of tissue engineered cartilage. *Biotechnol Bioeng*. **1999**; 63(2):197-205.

5) Stefan Jockenhoevel, Gregor Zund, Simon P. Hoerstrup, Khaled Chalabi, JoÈrg S. Sachweh, LuÈtfuÈ Demircan, Bruno J. Messmer, Marko Turina. Fibrin gel-advantages of a new scaffold in cardiovascular tissue engineering. *European Journal of Cardio-thoracic Surgery*,19 (**2001**); 424-430.

6) K. Jungermann and T Kietzmann. Oxygen: Modulator of Metabolic Zonation and Disease of the liver. *Hepatology.* **2000** Feb;31(2):255-60.

7) M. Celeste Simon1 & Brian Keith. The role of oxygen availability in embryonic development and stem cell function. *Nature Reviews Molecular Cell Biology* 9, 285-296 (April **2008**).

8) Preeti Malladi, Yue Xu, Michael Chiou, Amato J. Giaccia, and Michael T. Longaker. Effect of reduced oxygen tension on chondrogenesis and osteogenesis in adipose-derived mesenchymal cells. *Am J Physiol Cell Physiol*, **2006** Apr; 290(4): C1139-46.

9) Bojana Obradovic, Jerry H. Meldon, Lisa E. Freed, Gordana Vunjak-Novakovic. Glycosaminoglycan deposition in engineered cartilage: Experiments and mathematical model. *AIChE Journal*, Volume 46, Issue 9, pages 1860-1871, September **2000**.

10) Benjamin S. Harrison_, Daniel Eberli, Sang Jin Lee, Anthony Atala, James J. Yoo. Oxygen producing biomaterials for tissue regeneration. *Biomaterials* 28 (**2007**); 4628–4634.

11) Se Heang Oh, Catherine L. Ward, Anthony Atala, James J. Yoo, Benjamin S. Harrison. Oxygen generating scaffolds for enhancing engineered tissue survival. *Biomaterials* 30 (**2009**); 757–762.

12) Seifu DG, Isimjan TT, Mequanint K. Tissue engineering scaffolds containing embedded fluorinated-zeolite oxygen vector. *Acta Biomaterials* **2011** Oct; 7(10):3670-8.

13) Riess JG, Le Blanc M. Perfluoro compounds as blood substitutes. *Angew Chem Int Ed Engl* **1978**; 17:621-34.

14) Riess JG. Fluorocarbon-based in vivo oxygen transport and delivery systems. *Vox Sang* **1991**; 61:225-39.

15) Riess JG. The design and development of improved fluorocarbon-based products for use in medicine and biology. *Artif Cells Blood Substit Immobil Biotechnol* **1994**; 22:215-34.

16) Mitsuno T, Ohyanagi H. Present status of clinical studies of Fluosol-DA (20%) in Japan. *Int Anesthesiol Clin* **1985**;23:169-84.

17) Ingram DA, Forman MB, Murray JJ. Activation of complement by Fluosol attributable to the pluronic detergent micelle structure. *J Cardiovasc Pharmacol* **1993**; 22:456-61.

18) Hill SE, Leone BJ, Faithfull NS, Flaim KE, Keipert PE, Newman MF. Perflubron emulsion (AF0144) augments harvesting of autologous blood: a phase II study in cardiac surgery. *Cardiothorac Vasc Anest*, **2002**;16:555-60.

19) Faithfull NS. Mechanisms and efficacy of fluorochemical oxygen transport and delivery. *Artif Cells Blood Substit Immobil Biotechnol* **1994**; 22:181-97.

20) Toby A. Silverman and Richard B. Weiskopf for the Planning Committee and the Speakers. Hemoglobin-based oxygen carriers: current status and future directions. *Transfusion* Volume 49, November **2009**.

21) Reiter C, Wang X, Tanus-Santos J, Hogg N, Cannon R III, Schechter A, Gladwin M. Cell-free hemoglobin limits nitric oxide bioavailability in sickle-cell disease. *Nat Med.* **2002**; 8:1383–1389.

22) Olsen, J.S.; Foley, E.W.; Rogge, C.; Tsai, A.I.; Doyle, M.P.; Lemon, D.D. NO scavenging and the hypertensive effect of hemoglobin-based oxygen carriers. *Free Radic. Biol. Med.* **2004**, 36, 685-697.

23) Xiao C. Wu,W.J. Zhang,Ramaswami Sammynaiken,Qing H. Meng,Qiao Q. Yang,Eric Zhan,Qiang Liu,Wei Yang,Rui Wang. Non-functionalized carbon nanotube binding with hemoglobin. *Colloids and Surfaces B: Biointerfaces.* Volume 65, Issue 1, 1 August **2008**, Pages 146–149.

24) S Zong, Y Cao, Y Zhou, H Ju. Hydrogen peroxide biosensor based on hemoglobin modified zirconia nanoparticles-grafted collagen matrix. *Analytica Chimica Acta* Volume 582, Issue 2, 23 January **2007**, Pages 361–366.

25) Feng JJ, Zhao G, Xu JJ, Chen HY. Direct electrochemistry and electrocatalysis of heme proteins immobilized on gold nanoparticles stabilized by chitosan. *Anal Biochem.* **2005** Jul 15;342(2):280-6.

26) Su Young Chae, M.S., Sung Wan Kim, Ph.D., and You Han Bae, Ph.D. Effect of Cross-Linked Hemoglobin on Functionality and Viability of Microencapsulated Pancreatic Islets; *Tissue Engineering*, Volume 8, Number 3, **2002**; 379-394

27) Sakai H, Sou K, Horinouchi H, Kobayashi K, Tsuchida E. Review of Hemoglobin-Vesicles as Artificial Oxygen Carriers. *Artif Organs*. **2009** Feb; 33(2):139-45.

28) Quan Shi, Yubin Huang, Xuesi Chen, Meng Wu, Jing Sun, Xiabin Jing. Hemoglobin conjugated micelles based on triblock biodegradable polymers as artificial oxygen carriers. *Biomaterials* 30 (**2009**):5077–5085.

29) Robert R. Crichton, Stéphanie Wilmet, Rachida Legssyer, Roberta J. Ward Molecular and cellular mechanisms of iron homeostasis and toxicity in mammalian cells. *Journal of Inorganic Biochemistry*. Volume 91, Issue 1, 25 July **2002**, Pages 9‑18.

30) Ton That Hai, David E. Pereira,* and Deanna J. Nelson. Synthesis of Water-Soluble, Non-immunogenic Polyamide Cross-Linking Agents. *Bioconjugate Chem.* **1998**, 9, 645-654.

31) Matheson B, Kwansa H.E., Bucci E, Rebel A, Koehler R.C. Vascular response to infusions of a nonextravasating hemoglobin polymer. *J Appl Physiol* 93:1479-1486, **2002**.

32) J.M. Goddard, J.H. Hotchkiss. Polymer surface modification for the attachment of bioactive compounds. *Prog. Polym. Sci.* 32 (**2007**) 698–725.

33) Yang Zhu, Zhengwei Mao, Changyou Gao. Aminolysis-based surface modification of polyesters for biomedical applications. *RSC Adv.*, **2013**, 3, 2509-2519.

34) Greg T. Hermanson. Bioconjugate Techniques. *Elsevier Science (USA)*, **1996**, page 156.

35) Angela Guaccio, PhD Thesis. Il metabolismo cellulare in tessuti tridimensionali ingegnerizzati. **2005**.

36) Guaccio A, Borselli C, Oliviero O, Netti PA. Oxygen consumption of chondrocytes in agarose and collagen gels: a comparative analysis. *Biomaterials*. **2008** Apr; 29(10):1484-93.

37) J.M. Goddard, J.H. Hotchkiss. Polymer surface modification for the attachment of bioactive compounds. *Prog. Polym. Sci.* 32 (**2007**) 698–725.

38) Antonio Cittadini et al. Complementary therapeutic effects of dual delivery of insulin-like growth factor-1 and vascular endothelial growth factor by gelatin microbeads in experimental heart failure. *Eur J Heart Fail.* **2011** Dec; 13 (12):1264-74 22045926.

39) N. Adhirajana, N. Shanmugasundarama, S. Shanmuganathanb, Mary Babua. Functionally modified gelatin microbeads impregnated collagen scaffold as novel wound dressing to attenuate the proteases and bacterial growth. *European journal of pharmaceutical sciences* 3 6 (**2009**) 235–245.

40) Zenon Grabareka, John Gergelya. Zero-length crosslinking procedure with the use of active esters. *Analytical Biochemistry*; Volume 185, Issue 1, 15 February **1990**, Pages 131–135.

41) John P. Harrington and Hanna Wollocko. Molecular Design Properties of OxyVita Hemoglobin, a New Generation Therapeutic Oxygen Carrier: A Review; *J. Funct. Biomaterial*. **2011**, 2, 414-424

42) Jorge P. López-Alonso, Fernando Diez-García , Josep Font, Marc Ribó, Maria Vilanova, J. Martin Scholtz Carlos González, Francesca Vottariello, Giovanni Gotte, Massimo Libonati and Douglas V. Laurents. Carbodiimide EDC Induces Cross-Links That Stabilize RNase A C-Dimer against Dissociation: EDC Adducts Can Affect Protein Net Charge, Conformation, and Activity. *Bioconjugate Chem*., **2009**, 20 (8), 1459–1473.

43) Salvatore Magazu`, Emanuele Calabro` and Salvatore Campo. FTIR Spectroscopy Studies on the Bioprotective Effectiveness of Trehalose on Human Hemoglobin Aqueous Solutions under 50 Hz Electromagnetic Field Exposure. *J. Phys. Chem. B* **2010**, 114, 12144–12149.